

Targeting DNA Repair in Tumor Cells via Inhibition of ERCC1-XPF

Ahmed Elmenoufy, Francesco Gentile, David Jay, Feridoun Karimi-Busheri, Xiaoyan Yang, Olivier M Soueidan, Claudia Weilbeer, Rajam S Mani, Khaled H. Barakat, Jack Tuszynski, Michael Weinfeld, and F. G. West

J. Med. Chem., **Just Accepted Manuscript** • DOI: 10.1021/acs.jmedchem.9b00326 • Publication Date (Web): 01 Aug 2019

Downloaded from pubs.acs.org on August 2, 2019

Just Accepted

“Just Accepted” manuscripts have been peer-reviewed and accepted for publication. They are posted online prior to technical editing, formatting for publication and author proofing. The American Chemical Society provides “Just Accepted” as a service to the research community to expedite the dissemination of scientific material as soon as possible after acceptance. “Just Accepted” manuscripts appear in full in PDF format accompanied by an HTML abstract. “Just Accepted” manuscripts have been fully peer reviewed, but should not be considered the official version of record. They are citable by the Digital Object Identifier (DOI®). “Just Accepted” is an optional service offered to authors. Therefore, the “Just Accepted” Web site may not include all articles that will be published in the journal. After a manuscript is technically edited and formatted, it will be removed from the “Just Accepted” Web site and published as an ASAP article. Note that technical editing may introduce minor changes to the manuscript text and/or graphics which could affect content, and all legal disclaimers and ethical guidelines that apply to the journal pertain. ACS cannot be held responsible for errors or consequences arising from the use of information contained in these “Just Accepted” manuscripts.

Targeting DNA Repair in Tumor Cells via Inhibition of ERCC1-XPF

Ahmed H. Elmenoufy^{1,2}, Francesco Gentile³, David Jay⁴, Feridoun Karimi-Busheri⁴, Xiaoyan Yang⁴, Olivier M. Soueidan¹, Claudia Weilbeer¹, Rajam S. Mani⁴, Khaled H. Barakat⁵, Jack A. Tuszynski^{3,4}, Michael Weinfeld⁴ and Frederick G. West^{1*}

¹Department of Chemistry, University of Alberta, Edmonton, Alberta, Canada T6G 2G2

²Department of Pharmaceutical Chemistry, College of Pharmacy, Misr University for Science and Technology, 6th of October City, Egypt, P.O. Box: 77

³Department of Physics, University of Alberta, Edmonton, Alberta, Canada T6G 2E1

⁴Department of Oncology, Cross Cancer Institute, University of Alberta, Edmonton, Alberta, Canada T6G 1Z2

⁵Faculty of Pharmacy and Pharmaceutical Sciences, University of Alberta, Edmonton, Alberta, Canada T6G 2H1

Abstract

The ERCC1-XPF heterodimer is a 5'-3' structure-specific endonuclease, which plays an essential role in several DNA repair pathways in mammalian cells. ERCC1-XPF is primarily involved in the repair of chemically-induced helix-distorting and bulky DNA lesions, such as cyclobutane pyrimidine dimers (CPDs), and DNA interstrand crosslinks. Inhibition of ERCC1-XPF has been shown to potentiate cytotoxicity of platinum-based drugs and cyclophosphamide in cancer cells. In this study, the previously described ERCC1-XPF inhibitor 4-((6-chloro-2-methoxyacridin-9-yl)amino)-2-((4-methylpiperazin-1-yl)methyl)phenol (compound **1**) was used as a reference compound. Following the outcome of docking-based virtual screening (VS), we synthesized seven novel derivatives of **1** that were identified *in silico*

1
2 as being likely to have high binding affinity for the ERCC1-XPF heterodimerization interface by
3
4 interacting with the XPF double helix–hairpin–helix (HhH2) domain. Two of the new compounds, 4-((6-
5 chloro-2-methoxyacridin-9-yl)amino)-2-((4-cyclohexylpiperazin-1-yl)methyl)phenol (compound **3**) and
6
7 4-((6-chloro-2-methoxyacridin-9-yl)amino)-2-((4-(2-(dimethylamino)ethyl) piperazin-1-yl) methyl)
8
9 phenol (compound **4**), were shown to be potent inhibitors of ERCC1-XPF activity *in vitro*. Compound **4**
10
11 showed a significant inhibition of the removal of CPDs in UV-irradiated cells and the capacity to sensitize
12
13 colorectal cancer cells to UV radiation and cyclophosphamide.
14
15
16
17
18

19 **Introduction**

20
21
22 The ERCC1-XPF heterodimer is a critical DNA repair endonuclease. It plays a pivotal role in nucleotide
23
24 excision repair (NER) of bulky adducts and helix-distorting DNA lesions such as UV-induced
25
26 pyrimidine-(6,4)-pyrimidone photoproducts (6-4PPs) and CPDs¹⁻⁴. ERCC1-XPF is also involved in
27
28 DNA interstrand crosslink (ICL) repair⁵ in cells treated with platinum-based and other chemotherapeutic
29
30 agents such as cyclophosphamide and mitomycin C (MMC)⁶. In a recent study, 72% of colorectal cancer
31
32 patients showed positive ERCC1 protein expression which may be a useful marker for colorectal cancer
33
34 patients⁷. There is also evidence that ERCC1-XPF participates in DNA double-strand break (DSB) repair
35
36
37
38
39
40
41
42
43
44
45
46
47
48
49
50
51
52
53
54
55
56
57
58
59
60
It thus contributes significantly to the response of cancer cells to a range of DNA-damaging
chemotherapeutic agents and radiotherapy. In the ERCC1–XPF complex structure, ERCC1 is considered
to be catalytically inactive but rather regulates DNA–protein and protein–protein interactions, whereas
the endonuclease activity is provided by XPF, which also contains an inactive helicase-like motif that is
likely to be involved in protein–protein interactions and DNA binding^{10,11}.

ERCC1-XPF is an attractive target for drug design due to the availability of experimental structures and
the presence of multiple sites that can be inhibited with small molecules to stop the activity of the
endonuclease. Our earlier drug design studies focused on the XPA-ERCC1 interaction site¹² and the

1 XPF active site¹³, fostering the use of computer-aided drug design to develop DNA repair inhibitors¹⁴.
2
3
4 However, due to the specificity of the ERCC1-XPF interaction and its general involvement in all the
5
6 ERCC1-XPF mediated repair processes, the dimerization interface is perhaps the most promising domain
7
8 to target pharmacologically⁴. Dimerization and localization of ERCC1 and XPF is essential for the
9
10 enzyme's stability and endonuclease activity¹⁵. The dimerization of C-terminal regions of ERCC1 and
11
12 XPF is the key interaction to form a stable heterodimer. C-terminal regions dimerize through the
13
14 interaction of their double helix-hairpin-helix (HhH2) motifs^{16, 17}. It is thought that XPF acts as a
15
16 scaffold for ERCC1 during protein folding, and ERCC1 may exhibit improper folding *in vitro* in the
17
18 absence of XPF¹⁷. It was demonstrated that without dimerization the activity of ERCC1-XPF was
19
20 abolished because neither protein was stable, and therefore they were rapidly degraded^{18, 19}. As a result,
21
22 development of small molecule inhibitors that can disrupt the HhH2 domain interactions between ERCC1
23
24 and XPF would be expected to sensitize cancer cells to chemotherapeutic treatments whose DNA-
25
26 damaging effects are repaired by ERCC1-XPF-dependent pathways⁴. Moreover, rational drug design
27
28 methodology can be employed due to the availability of multiple experimental structures of the dimerized
29
30 HhH2 domains (for example, PDB code 2A1J and 1Z00)¹⁹.
31
32
33
34
35
36

37 Recently, McNeil *et al.* employed an *in-silico* screening approach targeting three sites on the XPF HhH2
38
39 domain to identify possible inhibitors for the dimer. They discovered a small molecule able to inhibit the
40
41 NER activity in melanoma cells and slightly sensitize them to cisplatin treatment. However, the reported
42
43 K_d and IC_{50} values for this compound were suboptimal, in the medium-high μM range²⁰. In addition,
44
45 Chapman *et al.*^{21, 22}, and Arora *et al.*²³ identified and optimized different small molecules targeting the
46
47 active site on the XPF nuclease domain. These efforts resulted in several endonuclease inhibitors with
48
49 IC_{50} in the nanomolar range, able to diminish NER activity and enhance the cytotoxicity of platinum-
50
51 based drugs in cancer cells. Although the specificity of these inhibitors to the ERCC1-XPF endonuclease
52
53 was assessed in some cases, similarities among active sites of various endonucleases could produce off-
54
55
56
57
58
59
60

1 target interactions from these compounds; the lack of structural insights of the ligand-protein complexes
2
3 in this case also limits further development of this series. Most recently, Yang *et al.* proposed the cellular
4
5 delivery of therapeutic peptides mimicking the ERCC1 HhH2 domain (residues 220-297) as a promising
6
7 alternative strategy to inhibit NER activity and sensitize cancer cells to DNA-damaging agents ²⁴.
8
9

10
11 Development of small molecule inhibitors of the HhH2 domain interaction would be expected to sensitize
12
13 cells to therapies whose DNA-damaging effects are repaired by ERCC1–XPF-dependent pathways.
14
15 Jordheim *et al.*, focused on developing small molecule inhibitors of the NER pathway acting through the
16
17 inhibition of ERCC1-XPF heterodimerization and reported that compound **1** (also called F06, NSC-
18
19 130813 or NERI02) interacted with XPF, repressed the interaction between ERCC1 and XPF *in vitro*
20
21 and sensitized cancer cells to MMC and cisplatin ²⁵. This affirms that targeting this protein-protein
22
23 interaction can enhance the cytotoxic activity of crosslinking agents such as cisplatin. The initial hit, **1**,
24
25 arose from a virtual screening (VS) of a large compound library, and the study also provided a
26
27 characterization of the XPF binding pocket and the binding mode of the compound to it ²⁵. Compound **1**
28
29 was predicted to interfere with the heterodimerization of ERCC1 and XPF, a necessary step to attain
30
31 DNA repair activity.
32
33
34
35
36
37

38 Preliminary *in-vitro* assays confirmed that **1** shows promising inhibitory activity and acts synergistically
39
40 with cisplatin. However, the activity of **1** is suboptimal in terms of clinical properties including potency
41
42 and safety, and a derivatization strategy, suggested by Jordheim *et al* ²⁵, was adapted to optimize the
43
44 action of the compound. Also, previous efforts on developing inhibitors for ERCC1-XPF activity were
45
46 carried out on the truncated version of the heterodimer, and not the full-length protein ^{2, 25-27}. It is reported
47
48 that the full length ERCC1–XPF protein was 15-fold more active than the truncated form under standard
49
50 reaction conditions ^{2, 19}. To the best of our knowledge, we are the first group to report inhibitors of the
51
52 activity of the full-length protein. Using **1** as a reference hit, we employed computer-aided drug design
53
54 techniques such as electrostatic mapping of the compound **1** binding pocket, molecular docking,
55
56
57
58
59
60

1 pharmacophore modeling and molecular dynamics (MD)-based rescoring to rank compound **1**
2 derivatives based on their predicted binding affinities to the XPF domain. The reference compound
3
4 (compound **1**) and top hits (compounds **2-7**) were synthesized and tested for their ability to inhibit the
5
6 *in-vitro* endonuclease activity of the full length ERCC1-XPF protein, and the most active compound was
7
8 further assessed as an inhibitor of the repair of UV-induced thymidine dimers in colorectal cancer cells,
9
10 as well as a sensitizing agent to not only to UV radiation but also to cyclophosphamide which has been
11
12 used to significantly reduce proliferation of metastatic colorectal cancer ²⁸.
13
14
15
16
17
18

19 **Results and Discussion**

20 Computer-aided drug design of compound **1** analogues

21
22
23
24
25
26 The first step was to investigate the binding mode of the hit compound, **1**, to the pocket on the XPF C-
27 terminus, followed by functionalization and extension of the piperazine ring in compound **1** : 1) provide
28 potential key interactions via hydrogen bond formation or hydrophobic interactions, and 2) optimize the
29
30 physicochemical properties and binding affinity for better potency and reduced toxicity of the compound
31
32
33
34
35 **1** based compounds.

36
37
38 The binding energy for the best docked conformation of **1** to the XPF structures was -10.23 kcal/mol, as
39
40 calculated by the Autodock scoring function. The compound showed a high shape complementarity with
41
42 the XPF pocket, which interacts with the F293 residue of ERCC1 in the dimerized complex (Figure S2A).
43
44 Three ligand-receptor hydrogen bonds were observed in the docked pose, namely with the side chain of
45
46 E829, the backbone of N834 and the backbone of K860. In addition, the hydrophobic core of **1**,
47
48 comprised of three aromatic rings, was positioned within a hydrophobic zone constituted by XPF residues
49
50 Y833, Q838, M856 and H857 (Figure S2B). Also, the binding mode of the ligand was in accordance
51
52 with the spatial distribution of the affinity maps calculated in Molecular Operating Environment 2015
53
54 (MOE2015) (Figure S2C).
55
56
57
58
59
60

1
2 To correctly place the scaffold common to all the analogues within the binding site, a pharmacophore
3
4 model based on the binding pose of **1** was built using MOE. This model included six features, namely
5
6 four aromatic moieties, one hydrogen bond donor, and one hydrogen bond acceptor features (Figure S2D
7
8 and Table S1 in Supporting Information). Upon generation of such features using MOE, we manually
9
10 adjusted their radii consistently with the spatial distribution of the affinity maps. The total number of
11
12 molecular structures that were docked was fifty-seven, accounting for all the different states generated
13
14 during the preparation step. After the docking was performed, just the top scored pose for each analog
15
16 was retained. The results were ranked according to their Generalized Born Volume Integral/Weighted
17
18 Surface Area (GBVI/WSA) score, as calculated by MOE. Then, we performed the MD simulations of
19
20 the complexes, and rescored the analogues using the Molecular Mechanics-Generalized Born Surface
21
22 Area (MM/GBSA) method. A subset of the top ranked hits was selected for chemical synthesis.
23
24
25
26
27

28 The results of the docking-based VS for this subset are reported in Table S2. The first two hits
29
30 (compounds **3** and **4**) were particularly interesting because of their binding energies in the range of the
31
32 lead compound, reasonable logP values and conserved ligand efficiencies with respect to the hit structure.
33
34 The decomposition of the binding energies among the residues of the binding pocket revealed a similar
35
36 pattern of ligand-receptor interactions for the compound **3**, **4** and **1**, although some differences are
37
38 noticeable for compound **4**.
39
40
41
42

43 The residues that contribute consistently to the binding of compound **1** analogues were identified as
44
45 Y833, M856, H857 and V859, where van der Waals interactions dominated the binding. Electrostatic
46
47 interactions were divided in highly-favorable with acidic residues (D823, E825, E829, E831, D839,
48
49 E864), and highly-unfavorable with basic residues (K832, K843, K850, R853, H857, H858, K860), due
50
51 in part to the positive protonation state of the piperazine ring of the compounds (Figure 1A). Noteworthy,
52
53 both contributions were generally higher for compound **4**, when compared with compound **1** and **3**. This
54
55 may be due to the addition of another positive R-substituent moiety in compound **4**, differently from and
56
57
58
59
60

1
2 compound **1** and **3** where hydrophobic groups were present as R-substituents. A further confirmation of
3
4 the different nature of the binding was found when analyzing the different contributions of the total
5
6 binding energy. Indeed, while **1** and compound **3** showed favorable electrostatic interactions, a highly-
7
8 unfavorable value was observed for compound **4**. An opposite trend was observed for the polar solvation
9
10 energy, highly-favorable for compound **4**, and highly-unfavorable for compound **1** and **3**. Van der Waals
11
12 and non-polar solvation contributions were similar for all the three compounds (Table S3). A detailed
13
14 analysis of the binding mode of compound **4** is shown in Figure 1B. The conserved core structure of the
15
16 analogue interacted similarly to **1** with the residues constituting the binding site, although the backbone
17
18 of V859 replaces K860 as hydrogen bond partner during the simulation. In addition, a network of water
19
20 molecules surrounding the binding site and interacting with the exposed R-substituent of compound **4**
21
22 was observed during the 2-ns simulation (Figure 1C). These water-ligand interactions may be responsible
23
24 for the favorable polar solvation contribution of the binding energy of compound **4**. Charge-charge
25
26 interactions with the E829 and E831 residues were maintained in terms of average magnitude, when
27
28 compared with **1**. Based on our simulations and because the branch containing the piperazine ring in **1** is
29
30 exposed to the solvent and cannot be accommodated in any additional cleft, we believe that adding a
31
32 hydrophilic extension such as for compound **4** strongly improves the ligand-solvent interactions.
33
34 Consistent with the importance of limiting the hydrophobicity of the piperazine ring extension,
35
36 compound **1** analogues carrying aromatic rings in their R-substituents showed reduced calculated binding
37
38 affinities (Table S2) and displayed inactivity in our incision assay (Figure 2). Importantly, charge-charge
39
40 interactions with E829 and E831 residues of XPF were maintained for compound **4**, when compared with
41
42
43
44
45
46
47
48 **1**.

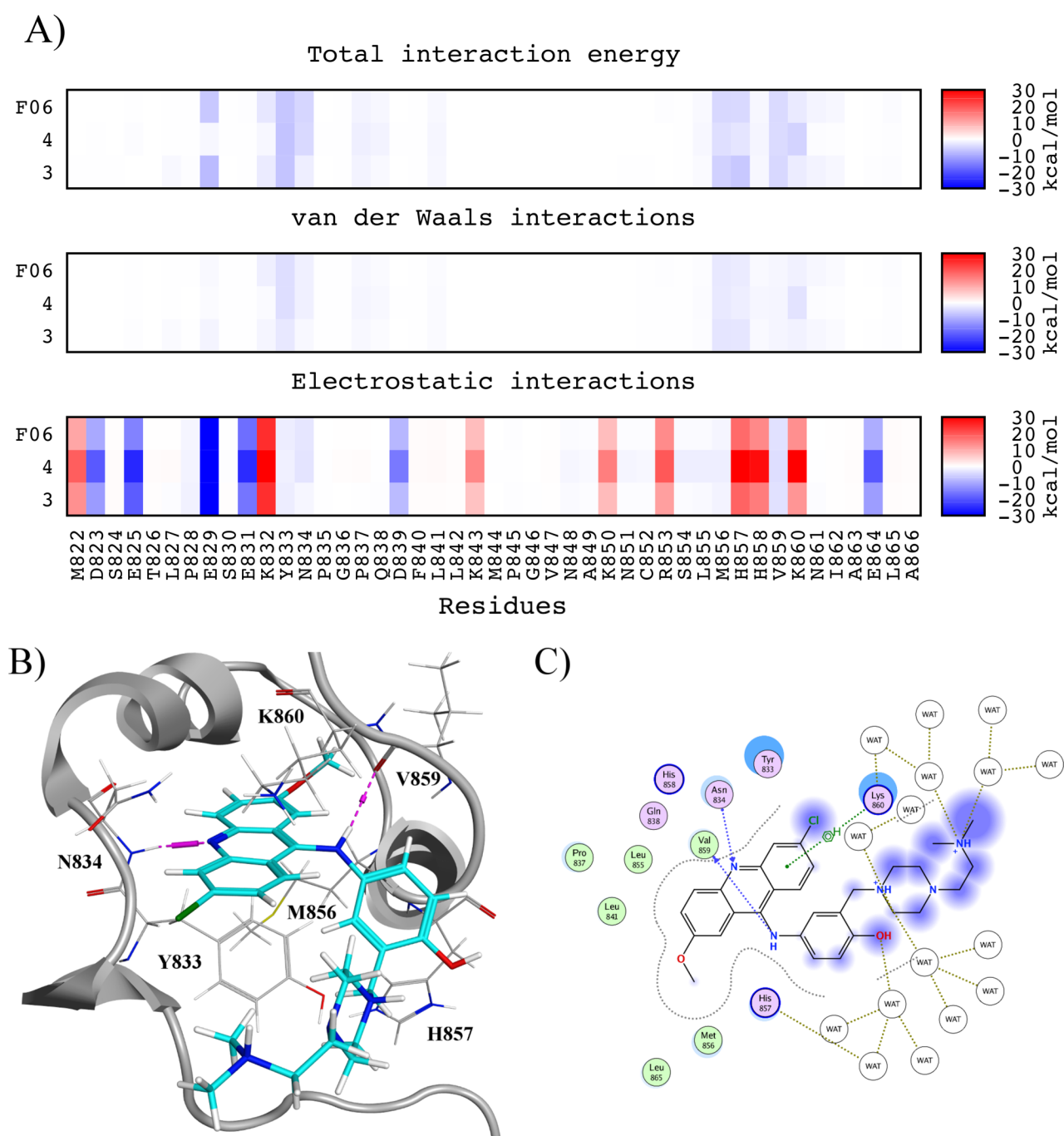


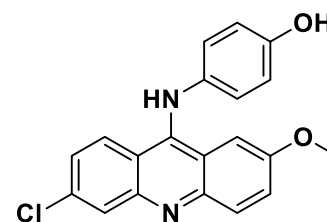
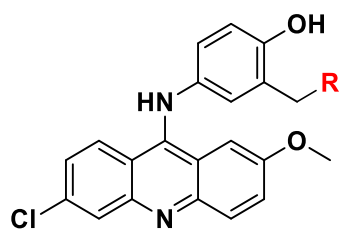
Figure 1. Analysis of the binding mode of the top hits. A) Per-residue decomposition of ligand-receptor binding energy. Compound 1 and 3 had similar patterns, while compound 4 showed a different pattern of interaction energies. Blue cells indicate favorable interactions, while red cells indicate unfavorable interactions. Refer to the text for more details. B) Lowest potential energy snapshot extracted from the MD simulation of compound 4 bound to XPF. Hydrogen bonds are colored in purple. The highest pocket

1
2 contributors in terms of total interaction energy are labelled. C) Interaction diagram for compound 4 and
3
4 surrounding residues and water molecules. The non-bonded interactions established with water
5
6 molecules was responsible for a highly-favorable polar solvation contribution to the binding energy. The
7
8 diagram refers to the lowest potential energy snapshot extracted from the MD simulation. Original PDB
9
10 structure for XPF: 1Z00.
11
12

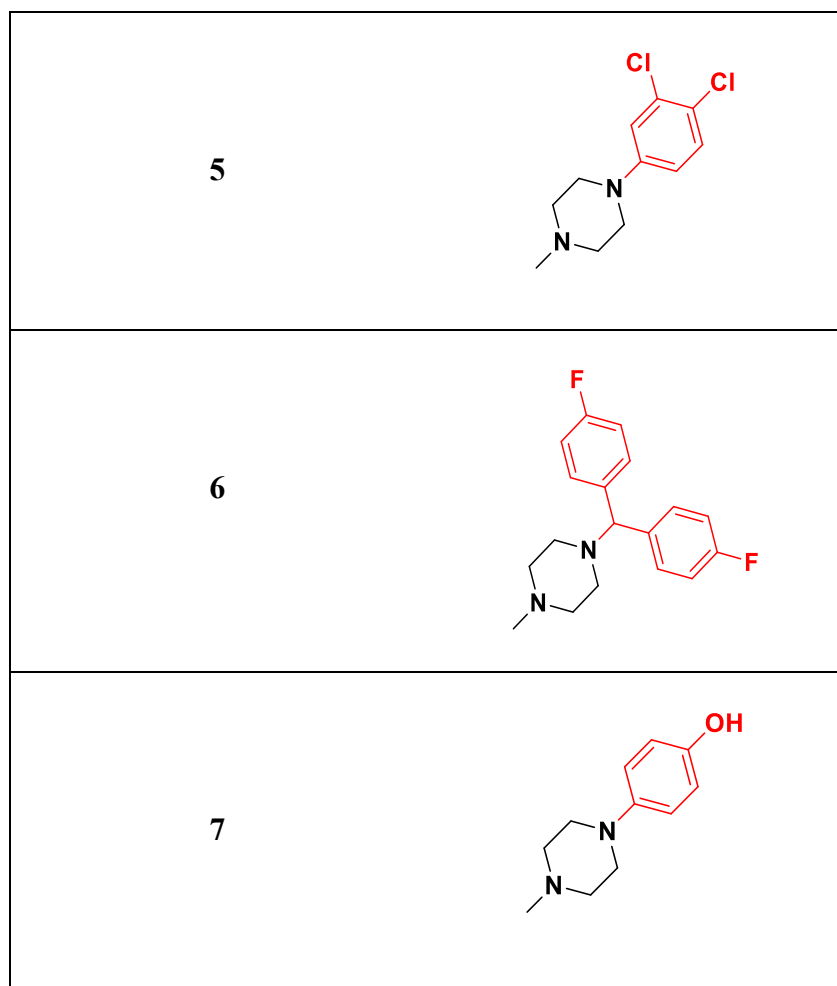
13 14 Synthesis of compound 1 based analogues 15

16
17 Synthesis of compounds **1-8** was achieved through a one-pot sequential addition reaction in 3 steps as
18
19 shown in Figure S1A. Mannich reaction of *p*-acetamidophenol with formaldehyde and appropriate
20
21 secondary amine in 2-propanol was carried out under reflux for 12 h. The solvent and excess of the
22
23 unreacted formaldehyde from the resulting mixture was removed under vacuum and without isolating
24
25 the compound, the resulting viscous residue was treated with 6 M HCl to deacetylate the acetamido group
26
27 to furnish the primary amine as depicted in Figure S1. Afterwards, an equimolar amount of 6,9-dichloro-
28
29 2-methoxyacridine was added, affording after heating compounds **1-8** in moderate to good yields after
30
31 isolation. The sequence is general, facile and reproducible. All synthesized compounds **1-8** were
32
33 characterized by ¹H NMR, ¹³C NMR, HRMS, IR and the purity of the most active compound 4 was
34
35 determined by HPLC (≥98% purity) as shown in page S32.
36
37
38
39
40

41
42 According to the *in-silico* screening, seven compounds were selected to be synthesized among the top
43
44 hits due to their promising ligand efficiencies and binding energy values in comparison to **1**.
45
46 Derivatization focused primarily on extension of the piperazine ring with different functionalities (i.e
47
48 alicyclic (compound **3**), substituted aromatics with electron donating (EDG) or electron withdrawing
49
50 (EWG) groups (compounds **2, 5, 6** and **7**), and an aliphatic chain installed with hydrogen bond acceptor
51
52 (HBA) atom (compound **4**) as shown in Table 1. Compound **8** was synthesized as a control to investigate
53
54 whether the piperazine ring is crucial for the activity of compounds.
55
56
57
58
59
60

Table 1.Compound 1 analogues functionalized with different R substituents.**Compound 8 (control)**

Compound	R
1 (reference)	
2	
3	
4	



Inhibition of ERCC1-XPF endonuclease activity

We used an *in-vitro* real-time fluorescence-based assay to assess the inhibitory effect of the synthesized compounds (except compound **2** due to its instability over time) on ERCC1-XPF endonuclease activity. This assay has been previously described²⁹, and utilizes a stem-loop substrate (composed of a 10mer-duplex stem and a 20mer-oligo dT single-strand loop), labelled on the 5'-terminus with 6-FAM and 3' with the quencher dabcyI. Upon ERCC1-XPF cleavage in the 10mer-duplex region an 8-base 5' FAM-labelled product is released resulting in an increased fluorescent signal (Figure 2A, Control). The other tracings in Figure 2A indicate to what extent the different compounds (10 μ M each) could inhibit scission of the substrate.

As shown here, three compounds exhibited a marked capacity to inhibit the nuclease activity of ERCC1-XPF, i.e. compounds **1**, **3** and **4**. For these three compounds, different concentrations of the drugs were plotted against the initial velocity (V_o , change in relative fluorescence units (RFU)/time) of the enzyme. Figure 2B (inset) shows an example of data obtained with compound **4**. Half-maximum inhibitory concentrations (IC_{50}) for these compounds were estimated from at least three different experiments for every compound (Table S4).

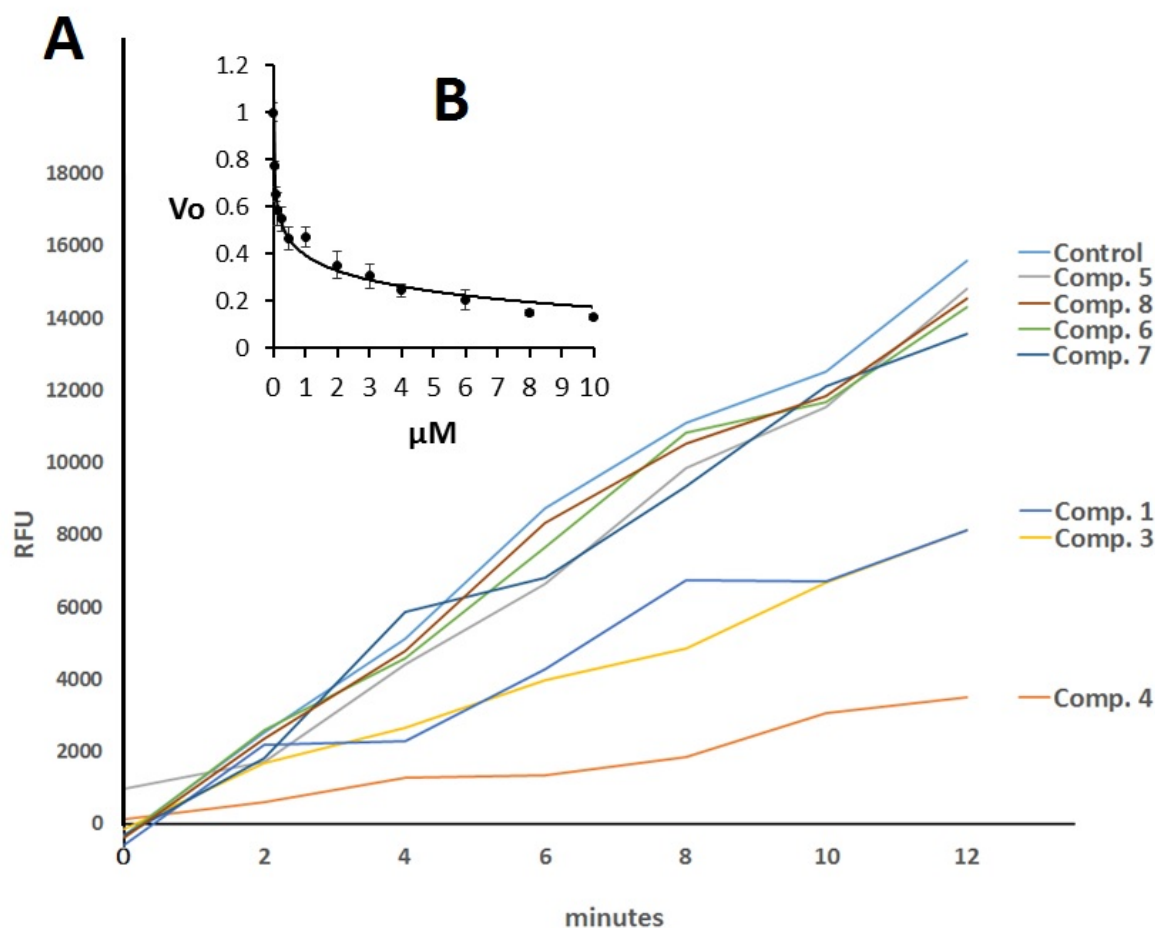


Figure 2. *In-vitro* inhibition of ERCC1-XPF endonuclease activity. A microplate fluorescent assay was used to measure inhibition of ERCC1-XPF endonuclease activity by the different compounds. Incubation of the DNA stem-loop substrate with ERCC1-XPF resulted in the release of a fluorescent 8-base fragment. A) Shows the increase in fluorescence (FRU) with time. A representative tracing of the effect

1
2 of the different compounds (8 μM each) on the incision activity is shown. B) (inset) shows a
3
4 representative plot of enzyme rate ($\Delta\text{RFU}/\text{time}$) vs compound 4 concentration.
5
6

7 Since acridine compounds are known to bind nucleic acids, the possibility existed that a disruption of the
8 structure of the stem-loop substrate by compound 4 could have been responsible for the inhibition
9 observed in the ERCC1-XPF kinetic assays. To rule out this possibility the experiment shown in Figure
10 S4 was carried out. Pre-incubation of ERCC1-XPF with compound 4 (3 μM) in the reaction medium
11 resulted in a time-dependent loss of enzyme activity. The reactions were started either with addition of
12 the substrate (**T0**) or with substrate that had been pre-incubated in the reaction medium in the presence
13 of compound 4 (3 μM) for 12 minutes (**T12**). The data indicate that the time-dependent inactivation of
14 ERCC1-XPF by compound 4 was the consequence of the interaction of the drug with the enzyme, and
15 not altered by addition of substrate that had been pre-incubated with the inhibitor. The data in Figure
16 S4A were obtained with a concentration of compound 4 approximately 9 times higher than the observed
17 IC_{50} value of the compound and in the presence of 10% DMSO. When the same test was carried out in
18 the presence of 5% DMSO, a similar time-dependent inhibition was observed and the substrate exhibited
19 comparable behavior (Figure S4B). (The IC_{50} values reported in the present study were obtained by
20 incubating ERCCI-XPF in the presence of the indicated concentrations of the drug for 30 minutes in the
21 reaction medium containing 5% DMSO.)
22
23
24
25
26
27
28
29
30
31
32
33
34
35
36
37
38
39
40
41
42

43 Inhibitor binding to ERCC1-XPF

44
45

46 Intrinsic fluorescence spectroscopy (of the protein tryptophan residues) was utilized to study the binding
47 affinity of compound 4 (active compound) and compound 5 (non-active compound) to ERCC1-XPF
48 (Figure 3). Addition of 2 μM of compound 5 had no significant effect on protein fluorescence and the
49 observed fluorescence quenching at 330 nm was only $3 \pm 1\%$, thus providing no evidence of any
50 interaction. In contrast, addition of compound 4 (2 μM) induced nearly $23 \pm 2\%$ quenching of protein
51
52
53
54
55
56
57
58
59
60

1
2 fluorescence at 330 nm, clearly indicating interaction of compound **4** with the ERCC1-XPF complex as
3
4 depicted in Figure 3B. Binding affinity (in terms of dissociation constant, K_d) of compound **4** for
5
6 ERCC1-XPF complex was determined by following fluorescence quenching (a measure of ligand
7
8 binding) as a function of ligand concentration. A representative plot of relative fluorescence intensities
9
10 versus the concentration of compound **4** is shown in Figure 3C (inset). Nonlinear regression analysis
11
12 (GraphPad Prism Software, San Diego, CA) of the binding data was carried out as described in our earlier
13
14 paper (41) and revealed a unimodal binding with a K_d value of 100 ± 5 nM as also shown in Table S4.
15
16 Interestingly, compound **4** has a high binding affinity fo ERCC1-XPF that is almost 20-fold greater
17
18 than its binding affinity to the DNA stem loop substrate used in the assay which has a unimodal binding
19
20 with a K_d value of 2.1 ± 0.1 μ M. This disparity in binding affinity strongly suggests that inhibition by **4**
21
22 results from its interaction with ERCC1-XPF rather than with the DNA substrate
23
24
25
26
27
28
29
30
31
32
33
34
35
36
37
38
39
40
41
42
43
44
45
46
47
48
49
50
51
52
53
54
55
56
57
58
59
60

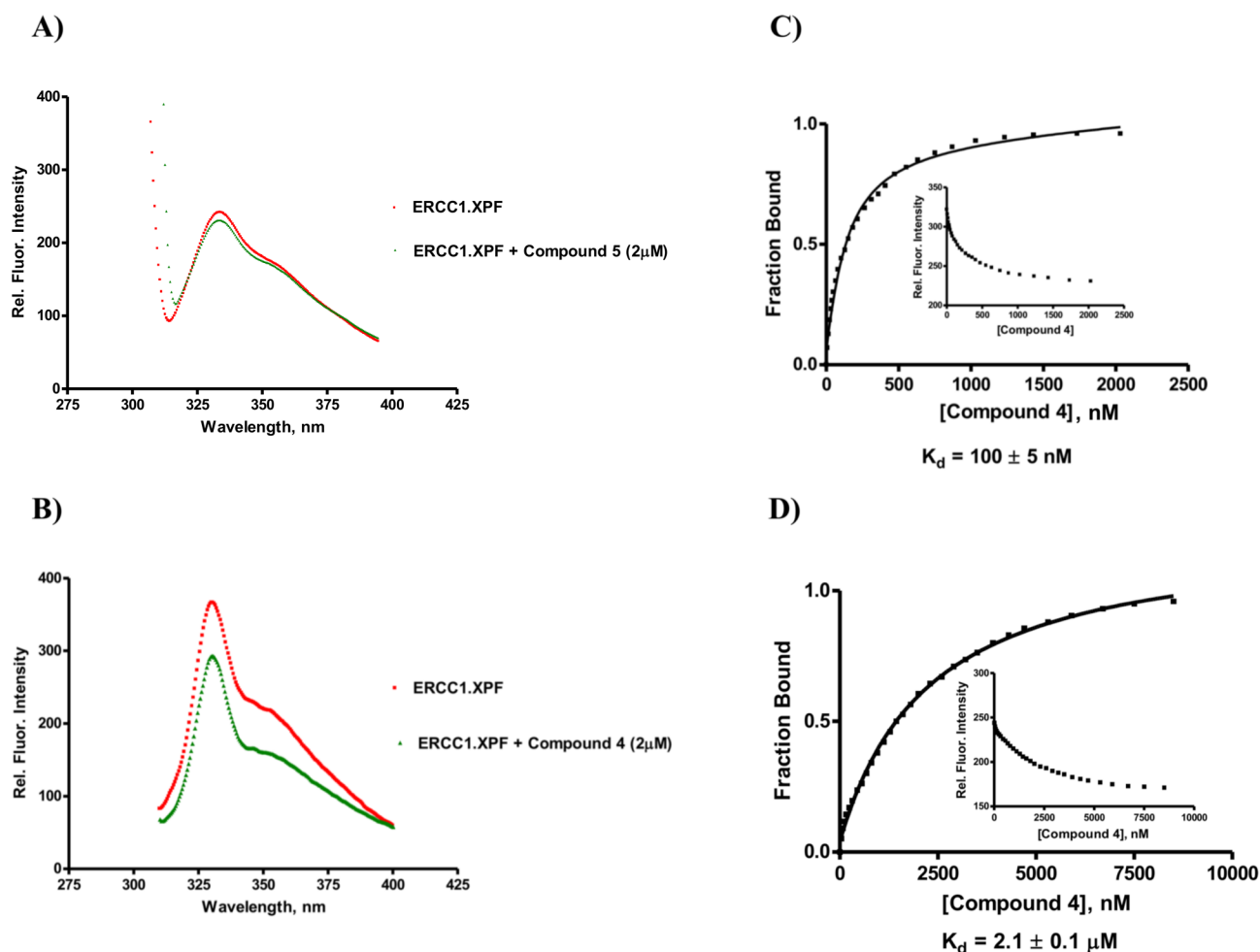


Figure 3. Determination of the affinity (K_d) between compound **4** and the ERCC1-XPF complex. Quenching of the intrinsic protein fluorescence of the tryptophan residues was used to monitor the interaction between the compounds and the protein. A) Fluorescence of ERCC1-XPF (13 nM and 20 nM) incubated with compound **5** (negative control), and B) compound **4** (active inhibitor) respectively. C) Unimodal binding pattern and the binding affinity of compound **4** with ERCC1-XPF (70 nM). The protein was excited at 295 nm and fluorescence intensity was monitored at 330 nm (see inset). The fraction bound (i.e. relative fluorescence) intensity versus ligand concentration is plotted. D) Binding of Compound **4** to DNA stem-loop substrate of ERCC1-XPF complex. The substrate of ERCC1-XPF was excited at 490 nm and the fluorescence intensity at 520 nm was monitored as a function of Compound **4**

1
2 concentration. A unimodal binding pattern was observed and the binding affinity of compound **4** to
3
4 ERCC1-XPF substrate was $2.1 \pm 0.1 \mu\text{M}$.
5

6
7 In an effort to identify a direct interaction between compound **4** and ERCC1-XPF we decided to utilize
8
9 microscale thermophoresis (MST) technique. We employed dERCC1 (ERCC1 codons 96-297) and
10
11 dXPF (XPF codons 667-916) for this analysis because these peptides contain the subunit interaction
12
13 domains that compound **4** was specifically designed to disrupt. Considering that dERCC1 is produced in
14
15 low yields in *E. coli* and dXPF, although highly expressed, is mainly generated as an insoluble fraction
16
17 in the absence of detergents². MST allows for the detection of interactions and changes in the molecular
18
19 properties of biomolecules at low nanomolar concentrations³⁰⁻³².
20
21

22
23 The expectation was that compound **4** would induce a larger change in the thermophoretic properties of
24
25 the truncated dimer as compared to each of the individual peptides provided the drug interacted with the
26
27 enzyme according to the proposed mechanism.
28

29
30 Figure S5 shows the thermophoretic property of the fluorescently labeled proteins in the presence or
31
32 absence of compound **4**. Initiation of the temperature gradient generated a depletion of the fluorescent
33
34 signal in the case of dXPF (grey line). In the case of dERCC1, after an initial depletion, the temperature
35
36 gradient induced a general accumulation of the fluorescent signal (light blue); a behavior that has been
37
38 observed before for other molecules³⁰. The dERCC1-dXPF dimer behaved in an intermediate fashion
39
40 (dark blue). Addition of compound **4** induced a reproducible minimal change in the dERCC1 (orange)
41
42 and dXPF (yellow) signals. Importantly, compound **4** changed more dramatically the signal of the
43
44 dERCC1-dXPF dimer (green vs dark blue), indicating that compound **4** interacts with ERCC1-XPF in
45
46 the subunit interaction domain and alters the properties of this region.
47
48

49 Inhibition of cellular repair of cyclobutane pyrimidine dimers

50
51
52
53 Significant inhibition of NER determined by the removal of UV-induced CPDs compared with control
54
55 cells over 24 hours is depicted in Figure 4. Immunofluorescent detection of CPDs after the exposure of
56
57
58

HCT-116 colorectal cells to 8 J/m^2 treated with compound **4** showed a significant inhibition of removal of CPDs compared with control cells over 24 hours. Based on our results and others³³, approximately 80% of CPDs are removed over 24 hours after UV exposure of HCT-116 cells, but this was reduced to approximately 60% in the presence of compound **4**. On the other hand, compound **5**, which demonstrated very limited inhibition *in vitro*, failed to inhibit the cellular removal of CPDs. Figure 4B shows the relative quantification of CPDs after treatment with active (**4**) and inactive (**5**) compounds.

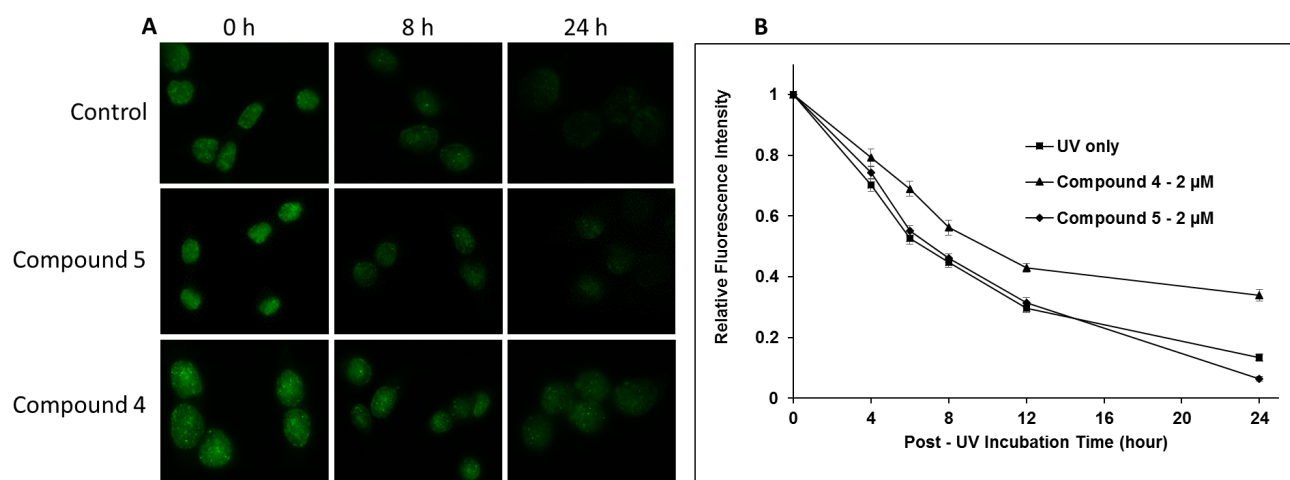


Figure 4. Inhibition of cellular NER. A) Immunofluorescence images of the UV-based assay for detecting CPDs in HCT-116 cells treated with compounds **4** and **5**. B) Normalized fluorescence intensity of the treated cells (\pm S.E.M) based on quantitation of fluorescence from 50 randomly selected cells per treatment. All the values obtained for treatment with compound **4** from 4-24 h post-irradiation were significantly different ($p < 0.005$, Student's t-test) from the values obtained with the control irradiated cells.

Increased sensitization to UV radiation and cyclophosphamide

We also evaluated the effectiveness of compound **4** (1 and 2 μM non-cytotoxic doses were chosen according the clonogenic survival assay of compound **4** as shown in Figure S3) to sensitize cells to UV

irradiation based on clonogenic survival as shown in Figure 5A. In accord with the repair data, 2 μM compound **4** significantly reduced survival of the UV irradiated cells.

We then examined the combined effect of compound **4** (1 and 2 μM) on cellular survival following exposure to the DNA interstrand crosslinking agent cyclophosphamide using HCT 116 (WT) cells and XPF knockout cell lines. The survival curves shown in Figure 5B indicate that, at a concentration of 2 μM , compound **4** significantly sensitized the cells to cyclophosphamide (starting at 50 μM) and no colonies were detected on the plates with a cyclophosphamide concentration of 300 μM .

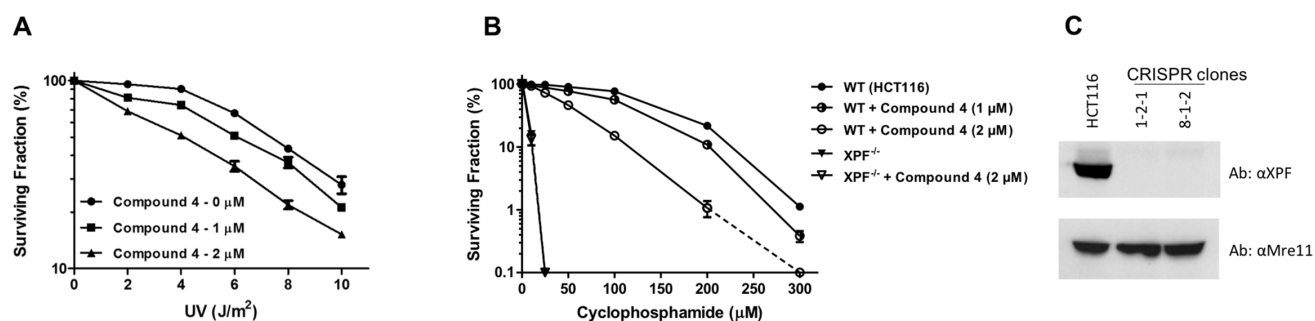


Figure 5. Sensitization of cells to UV and cyclophosphamide. A) Survival of HCT-116 cells exposed to increasing doses of 254 nm UV radiation and treated with 1 and 2 μM compound **4** determined by the clonogenic survival assay. B) Survival of HCT-116 cells exposed to increasing doses of cyclophosphamide and treated with 1 and 2 μM compound **4** determined by the clonogenic survival assay. The dashed line indicates that the no colonies were observed after treatment with 300 μM cyclophosphamide + 2 μM compound **4**. The survival curves (\pm S.E.M) are based on three independent sets of determinations. All the values obtained with cells treated with 2 μM compound **4** were significantly different ($p < 0.005$, Student's t-test) from the values obtained with the control cells not treated with compound **4**. C) Human XPF gene knock out confirmation on two positive clone 1-2-1 and 8-1-2 by Western blot analysis using monoclonal antibodies against XPF and Mre11, as control proteins.

Pharmacokinetic properties of Compound **4** and compound **1**

1 Parental compound **1** of our lead compound **4** was submitted to WuXi AppTec (Shanghai) Co.⁴⁴ in China
2
3
4 to further investigate the ADME profile of the two compounds and compare their results to know whether
5
6 compound **4** is pharmacokinetically more superior than compound **1**. Compound **4** showed a lower LogD
7
8 (2.86) than **1** (3.86) at pH 7.4 (Table S5). Metabolism of compound **4**, as measured by human liver
9
10 microsome indicated that it has a metabolism in the mid-range, while **1** has a more rapid metabolism.
11
12 Both compounds display an efflux ratio of higher than 2 (compound **4** = 8.92 and compound **1** = 11.18).
13
14 Analysis of five CYP 450 tested enzymes indicates that neither of the compounds has an IC₅₀ lower than
15
16 1.00 μM therefore they are not potent inhibitors of these enzymes. Compound **4**, however, moderately
17
18 inhibits CYP1A2 with an IC₅₀ of 6.40 μM. Compound **1** has the same moderate inhibitory effect on
19
20 CYP2D6 and CYP3A4-M with an IC₅₀ between 1 to 10 μM. Compound **4** acts as a weak inhibitor of
21
22 CYP2D6 and CYP3A4-M while **1** is a weak inhibitor of three CYP 450 enzymes (CYP1A2, CYP2C9,
23
24 and CYP2C19) with an IC₅₀ between 10 to 50 μM. Both compounds have similar behavior in terms of
25
26 permeability and binding to serum proteins as shown in Table S5.
27
28
29
30

31 To conclude, our comparison of the ADME results between **1**, the parental compound, and compound **4**
32
33 indicated that the latter has more favourable pharmacological properties, particularly a lower LogD than
34
35 **1**, which means that it has a lower lipophilicity, and greater metabolic stability.
36
37
38
39

40 Conclusion

41
42 The ERCC1-XPF heterodimer is a structure-specific endonuclease, which is required especially for NER
43
44 and ICL DNA repair pathways. Although its action is essential to maintain genome integrity and to
45
46 protect against damage-induced mutations, as part of the NER and ICL machinery it can counteract the
47
48 effect of DNA damaging therapies such as platinum-based chemotherapy and radiotherapy. A promising
49
50 approach to enhance the effect of such therapies is to inhibit the action of DNA repair in cancer cells
51
52 using small molecules. In this work, we used a computational drug design workflow to provide a rational
53
54 design for novel compound **1** analogues, a lead inhibitor targeting the dimerization between XPF and
55
56
57
58
59
60

1 ERCC1, which is required for endonuclease activity. We identified seven compounds for which *in-silico*
2
3
4 simulations predicted attractive properties, namely binding affinities and ligand efficiency towards an
5
6 XPF site on the dimerization interface. The synthesis of the computationally designed compounds was
7
8 successfully carried out using a simple, robust and reproducible synthetic strategy. Interestingly,
9
10 compound **4** has good physicochemical properties, i.e. reasonable logP and ligand efficiency values, and
11
12 small molecular weight (see Table S4), and thus is a potential lead candidate for further optimization.
13
14 Following structure-activity relationship studies and *in-vitro* screening, this approach yielded compounds
15
16 **3** and **4** as potent inhibitors of ERCC1-XPF activity. An *in-vitro* ERCC1-XPF endonuclease assay
17
18 identified compound **4** as the best ERCC1-XPF inhibitor with an IC₅₀ value of 0.33 μM compared to
19
20 1.86 μM for **1**. In addition, the K_d value for this compound was experimentally measured as 100 nM and
21
22 interacts with ERCC1-XPF in the subunit interaction domain and alters the related properties of this
23
24 heterodimerization interface. Compound **4** also showed a significant inhibition of the removal of
25
26 cyclobutane pyrimidine dimers compared with control cells after exposure of HCT-116 cells to UV
27
28 radiation and sensitized the cells to UV and cyclophosphamide-induced cytotoxicity, indicating
29
30 inhibition of NER and ICL repair. Furthermore, compound **4** possesses favourable pharmacokinetic
31
32 properties, particularly a lower LogD than compound **1**, which means that it has a lower lipophilicity,
33
34 and greater metabolic stability. Our computational workflow successfully identified superior compounds
35
36 from a set of analogues differing by one substituent group. Additionally, it provided detailed information
37
38 about the ligand-protein interaction. Compound **4** was our best *in vitro* analogue. Detailed analysis of the
39
40 MM/GBSA binding energies, together with the visual analysis of the simulation results, suggests a
41
42 binding mode for compound **4** where the conserved hydrophobic core of the analogue is buried inside
43
44 the XPF binding site and, differently to the other active compounds (**1** and **3**) the positive R-substituent
45
46 is favorably exposed to the solvent. Although all of the compounds share the acridine moiety, our assay
47
48 showed that the inhibition activity of compound **4** was the consequence of the interaction of the drug
49
50 with the enzyme, and not the result of binding with DNA. The fact that compounds **4** and **5** (negative
51
52
53
54
55
56
57
58
59
60

control) show drastically different activity despite possessing the same acridine moiety also provides strong evidence that inhibition is not mediated via DNA intercalation. In future work, compound **4** will be the starting point for further optimization towards a drug candidate compound to yield an optimized lead analogue of compound **4**. Since polar side-chain installation at the exterior part of the piperazine position clearly enhances activity, we intend to explore a wider range of polar groups on the remote end of the piperazine. At the same time, we will retain the dimethylaminoethyl group and explore structural changes in parts of the molecule that are more deeply intercalated into the protein binding pocket. Different generation of compound **4** derivatives will be synthesized according to the corresponding *in silico* studies and the current SAR results in this study for the aim of obtaining a drug like candidate that has superior physicochemical properties than compound **4**. In summary, the use of *in-silico* methods to design a superior compound to **1** led to compound **4** that can potentially be used in combination with other existing DNA-damaging therapies to amplify their effects by sensitizing cancer cells.

Methods and Experimental section

General experimental procedures for preparation of the top compound **1** analogues

Synthesis and characterization of compounds **1-8** are described in Supporting Information, section 6. Reactions were carried out in flame-dried glassware under a positive argon atmosphere unless otherwise stated. Transfer of anhydrous solvents and reagents was accomplished with oven-dried syringes or cannulae. Solvents were distilled before use. Chemicals were purchased from Sigma Aldrich Inc., and were used without further purification. Thin layer chromatography was performed on glass plates pre-coated with 0.25 mm silica gel. Flash chromatography columns were packed with 230-400 mesh silica gel. Proton nuclear magnetic resonance spectra (^1H NMR) were recorded at 500 MHz, and coupling constants (J) are reported in hertz (Hz). Standard notation was used to describe the multiplicity of signals observed in ^1H NMR spectra: broad (br), multiplet (m), singlet (s), doublet (d), triplet (t), etc. Carbon

nuclear magnetic resonance spectra (^{13}C NMR) were recorded at 125 MHz and are reported (ppm) relative to the center line of the triplet from chloroform-d (77.0 ppm) or the center line of the heptuplet from methanol-d₄ (49.0 ppm). Infrared (IR) spectra were measured with a FT-IR 3000 spectrophotometer. Mass spectra were determined on a high-resolution electrospray positive ion mode spectrometer. The high-performance liquid chromatography (HPLC) analyses were performed using a Agilent 1100 LC/MSD instrument. Elution was done with a gradient of 10–95% solvent B in solvent A (solvent A was 0.1% TFA in water, and solvent B was 0.1% acetic acid in MeCN) through an Agilent column eclipse XDB- C18 (4.6× 250 mm, 5 μm) column at 1.0 mL/min. Area % purity was measured at 210 and 254 nm. The purity of the most active compound was assessed by HPLC (>95%).

Synthesis and characterization of inhibitors (1-8)

4-((6-Chloro-2-methoxyacridin-9-yl)amino)-2-((4-methylpiperazin-1-yl)methyl)phenol (1)

Synthesis of compound **1** was achieved through one pot sequential addition reaction in 3 steps. A mixture of *N*-methyl piperazine (0.12 mL, 1.0 mmol), acetaminophen (0.15 g, 1.0 mmol) and 37% formaldehyde (0.10 mL, 5 mmol) in isopropyl alcohol (2 ml) was taken in 10 mL single neck round bottom flask. Then, the reaction mixture was stirred and heated under reflux at 65 °C for 6 h. Upon completion of the reaction (monitored by TLC with 15% MeOH/DCM eluent system), the solvent was removed on a rotatory evaporator. Next, the residue was dissolved in 3 mL ethanol and 3 drops of 12 *M* HCl were added. Subsequently, the reaction mixture was heated at 90 °C under reflux for 90 min. Afterwards, 6,9-dichloro-methoxyacridine (0.28 g, 1.0 mmol) was added to the mixture and further stirred at 90 °C under reflux and the course of reaction followed by TLC until little or no starting material was detected (around 12 h). On cooling to room temperature, the reaction mixture was diluted with cold water and neutralized to pH of 8-9 with 28% v/v ammonia solution. The alkaline solution was extracted with dichloromethane. The organic layer was washed with brine, concentrated in vacuum, and purified by column chromatography (gradient elution with 5% to 10% MeOH:DCM system) to afford compound **1** as orange reddish semisolid (0.08 g) in 78 % yield; R_f 0.50 (2:8, MeOH:DCM); IR (cast film) ν_{max} = 3272, 2923, 1629, 1254, 1231, 1032, 926, 816, 815, 775 cm^{-1} ; ^1H NMR (500 MHz, CDCl_3) δ 7.99 (s, 1H), 7.91 (d, J = 8.7 Hz, 1H), 7.80 (d, J = 9.2 Hz, 1H), 7.29 (dd, J = 9.4, 2.6 Hz, 1H), 7.11 (d, J = 10.7 Hz, 1H), 7.03 (s, 1H), 6.77 – 6.70 (m, 2H), 6.49 (d, J = 2.5 Hz, 1H), 3.63 (s, 3H), 3.53 (s, 2H), 2.75 – 2.32 (m, 8H), 2.27

(s, 3H), OH and NH protons were not observed; ^{13}C NMR (125 MHz, CDCl_3) δ 155.9, 153.2, 147.8, 143.9, 137.0, 135.0, 125.0, 124.9, 122.0, 121.8, 120.0, 119.9, 119.7, 117.61, 116.8, 116.5, 116.1, 115.9, 100.3, 61.1, 55.2, 54.8 (2C), 52.4 (2C), 45.8; HRMS (ESI) calcd for $\text{C}_{26}\text{H}_{28}\text{ClN}_4\text{O}_2$ $[\text{M} + \text{H}]^+$ 463.1895; found 463.1890.

4-((6-Chloro-2-methoxyacridin-9-yl)amino)-2-((4-(3-methylbenzyl)piperazin-1-yl)methyl)phenol (2)

The previous method was employed to synthesize compound 2 with the following stoichiometric amounts; 1-(3-methylbenzyl)piperazine (0.19 g, 1.0 mmol) and 6,9-dichloroacridine (0.28 g, 1.0 mmol) to afford it as orange reddish semisolid (0.14 g) in 73 % yield; R_f 0.44 (1:9, MeOH:DCM); IR (cast film) ν_{max} = 3258, 2921, 1629, 1560, 1493, 1253, 1133, 1007, 927, 826, 775 cm^{-1} ; ^1H NMR (500 MHz, CDCl_3) δ 8.05 (s, 1H), 7.95 (d, J = 9.2 Hz, 1H), 7.83 (d, J = 9.2 Hz, 1H), 7.32 (d, J = 7.6 Hz, 1H), 7.21 (t, J = 7.5 Hz, 1H), 7.17 – 7.06 (m, 5H), 6.87 (d, J = 7.1 Hz, 1H), 6.77 (d, J = 8.6 Hz, 1H), 6.62 (d, J = 1.9 Hz, 1H), 3.70 (s, 3H), 3.59 (s, 2H), 3.49 (s, 2H), 2.79 – 2.40 (m, 8H), 2.35 (s, 3H). OH and NH protons were not observed; ^{13}C NMR (125 MHz, CDCl_3) δ 156.1, 153.9, 150.4, 146.8, 144.5, 137.9, 137.6, 136.3, 135.5, 129.9, 128.2, 127.9, 126.2, 125.4, 125.0, 122.1, 121.8, 120.6, 120.3, 119.2, 116.9, 116.5, 116.1, 115.9, 100.4, 62.8, 61.2, 55.4, 52.8 (2C), 52.5 (2C), 21.4; HRMS (ESI) calcd for $\text{C}_{33}\text{H}_{34}\text{ClN}_4\text{O}_2$ $[\text{M} + \text{H}]^+$ 553.2357; found 553.2365.

4-((6-Chloro-2-methoxyacridin-9-yl)amino)-2-((4-cyclohexylpiperazin-1-yl)methyl)phenol (3)

The previous method was employed to synthesize compound 3 with the following stoichiometric amounts; 1-cyclohexyl piperazine (0.17 g, 1.0 mmol) and 6,9- dichloroacridine (0.28 g, 1.0 mmol) to afford it as orange reddish semisolid (0.13 g) in 81 % yield; R_f 0.52 (0.5:9.5, MeOH: EtOAc); IR (cast film) ν_{max} = 3313, 2918, 1736, 1560, 1468, 1255, 1235, 1181, 1032, 929, 829, 722 cm^{-1} ; ^1H NMR (500 MHz, CDCl_3) δ 8.03 (d, J = 1.4 Hz, 1H), 7.92 (d, J = 9.6 Hz, 1H), 7.80 (d, J = 9.5 Hz, 1H), 7.28 (d, J = 5.7 Hz, 1H), 7.11 (d, J = 9.1 Hz, 2H), 6.91 (d, J = 9.3 Hz, 1H), 6.77 (d, J = 8.5 Hz, 1H), 6.69 (s, 1H), 3.71 (s, 3H), 3.60 (s, 2H), 2.73 – 2.22 (m, 8H), 1.83 (m, 4H), 1.63 (d, J = 12.8 Hz, 1H), 1.26 – 1.18 (m, 6H). OH and NH protons were not observed; ^{13}C NMR (125 MHz, CDCl_3) δ 156.1, 153.8, 146.9, 144.5, 136.3, 135.5, 125.4 – 116.8 (10 C), 101.3, 100.4, 98.8, 63.4, 61.3, 52.9 (2 C), 48.7 (2 C), 29.7, 28.9 (2 C), 26.2, 25.8 (2 C); HRMS (ESI) calcd for $\text{C}_{31}\text{H}_{35}\text{ClN}_4\text{O}_2$ $[\text{M} + \text{H}]^+$ 531.2521; found 531.2527.

4-((6-Chloro-2-methoxyacridin-9-yl)amino)-2-((4-(2-(dimethylamino)ethyl) piperazin-1-yl) methyl) phenol (4)

1
2 The previous method was employed to synthesize compound 4 with the following stoichiometric
3 amounts; 1-[2-(dimethylamino)ethyl] piperazine (0.16 g, 1.0 mmol) and 6,9-dichloroacridine (0.28 g, 1.0
4 mmol) to afford it as orange reddish semisolid (0.13 g) in 80 % yield; R_f 0.40 (1.3: 8.5: 0.2, MeOH:
5 DCM: Et₃N); IR (cast film) ν_{\max} = 3361, 2918, 1736, 1562, 1467, 1295, 1255, 1143, 1032, 945, 828, 763,
6 722 cm⁻¹; ¹H NMR (500 MHz, CDCl₃) δ 8.10 (s, 1H), 8.00 (s, 1H), 7.89 (d, J = 9.1 Hz, 1H), 7.40 (d, J =
7 9.8 Hz, 1H), 7.24 (d, J = 8.0 Hz, 1H), 7.09 (s, 1H), 6.85 (dd, J = 8.6, 2.7 Hz, 1H), 6.78 (d, J = 8.6 Hz,
8 1H), 6.56 (d, J = 2.3 Hz, 1H), 3.74 (s, 3H), 3.59 (s, 2H), 2.70 – 2.40 (m, 12H), 2.27 (s, 6H). OH and NH
9 protons were not observed; ¹³C NMR (125 MHz, CDCl₃) δ 156.2, 153.6, 147.5, 144.0, 136.6, 135.2,
10 125.3, 125.1, 124.8, 122.0, 120.3, 120.2, 120.0, 119.8, 119.6, 117.5, 116.9, 116.3, 100.2, 61.2, 56.7, 56.7,
11 55.3, 53.3 (2C), 52.4 (2C), 45.8 (2C); HRMS (ESI) calcd for C₂₉H₃₅ClN₅O₂ [M + H]⁺ 520.2474; found
12 520.2473.
13
14
15
16
17
18
19
20
21

22 ***4-((6-Chloro-2-methoxyacridin-9-yl)amino)-2-((4-(3,4-dichlorophenyl)piperazin-1-yl)methyl)phenol***
23 **(5)**
24
25

26 The previous method was employed to synthesize compound 5 with the following stoichiometric
27 amounts; 1-(3,4-dichlorophenyl) piperazine (0.23 g, 1.0 mmol), acetaminophen (0.15 g, 1.0 mmol), 37%
28 formaldehyde (0.10 mL, 5 mmol) and 6,9- dichloroacridine (0.28 g, 1.0 mmol) to afford it as orange
29 reddish semisolid (0.16 g) in 71 % yield; R_f 0.56 (0.5:9.5, MeOH:DCM); IR (cast film) ν_{\max} = 3271,
30 2918, 1736, 1563, 1227, 1180, 1080, 1031, 803, 721 cm⁻¹; ¹H NMR (500 MHz, CDCl₃) δ 8.09 (s, 1H),
31 8.00 (s, 1H), 7.88 (d, J = 9.2 Hz, 1H), 7.40 (d, J = 9.3 Hz, 1H), 7.28 (d, J = 8.7 Hz, 1H), 7.24 (d, J = 9.0
32 Hz, 1H), 7.09 (s, 1H), 6.95 (d, J = 2.8 Hz, 1H), 6.87 (dd, J = 8.6, 2.7 Hz, 1H), 6.80 (d, J = 8.6 Hz, 1H),
33 6.73 (dd, J = 8.9, 2.8 Hz, 1H), 6.54 (d, J = 2.6 Hz, 1H), 3.74 (s, 3H), 3.63 (s, 2H), 3.27 – 3.15 (m, 4H),
34 2.72 – 2.62 (m, 4H), OH and NH protons were not observed; ¹³C NMR (125 MHz, CDCl₃) δ 156.3,
35 153.1, 150.2, 147.9, 143.3, 137.0, 135.0, 132.9, 130.5, 125.2, 124.7, 122.9, 121.6, 121.4, 120.2, 120.0,
36 119.7, 117.9, 117.6, 117.0, 116.7, 116.2, 115.6, 115.5, 100.0, 61.2, 55.4 (2C), 52.2 (2C), 48.7; HRMS
37 (ESI) calcd for C₃₁H₂₈Cl₃N₄O₂ [M + H]⁺ 593.1272; found 593.1272.
38
39
40
41
42
43
44
45
46
47

48 ***2-((4-(Bis(4-fluorophenyl)methyl)piperazin-1-yl)methyl)-4-((6-chloro-2-methoxyacridin-9-***
49 ***yl)amino)phenol (6)***
50
51

52 The previous method was employed to synthesize compound 6 with the following stoichiometric
53 amounts; 1-bis (4-fluorophenyl)methylpiperazine (0.29 g, 1.0 mmol), acetaminophen (0.15 g, 1.0 mmol),
54 37% formaldehyde (0.10 mL, 5 mmol) and 6,9- dichloroacridine (0.28 g, 1.0 mmol) to afford it as orange
55
56
57
58
59
60

reddish semisolid (0.19 g) in 65 % yield; R_f 0.56 (0.5:9.5, MeOH:DCM); IR (cast film) ν_{\max} = 3275, 2919, 1737, 1566, 1255, 1217, 1181, 1032, 828, 722 cm^{-1} ; ^1H NMR (500 MHz, CDCl_3) δ 8.07 (s, 1H), 7.98 (d, J = 9.0 Hz, 1H), 7.84 (d, J = 9.2 Hz, 1H), 7.34 (m, 6H), 7.18 (d, J = 8.0 Hz, 1H), 7.06 (d, J = 1.8 Hz, 1H), 6.97 (m, 5H), 6.83 (dd, J = 8.5, 2.6 Hz, 1H), 6.75 (d, J = 8.6 Hz, 1H), 6.53 (d, J = 2.2 Hz, 1H), 4.23 (s, 1H), 3.69 (s, 3H), 3.57 (s, 2H), 2.74 – 2.21 (m, 8H); ^{13}C NMR (125 MHz, CDCl_3) δ 161.9 (2C), 156.2, 153.5, 150.3, 147.7, 143.7, 137.8 (2C), 136.7, 135.0, 129.2 (4C), 125.2, 124.8, 121.9, 121.7, 120.2, 119.9, 119.7, 117.6, 116.8, 116.5, 116.1, 115.5 (4C), 100.0, 74.3, 61.1, 55.3, 52.6 (2C), 51.5 (2C); HRMS (ESI) calcd for $\text{C}_{38}\text{H}_{34}\text{ClF}_2\text{N}_4\text{O}_2$ $[\text{M} + \text{H}]^+$ 651.2333; found 651.2328.

4-((6-Chloro-2-methoxyacridin-9-yl)amino)-2-((4-(4-hydroxyphenyl)piperazin-1-yl)methyl)phenol (7)

The previous method was employed to synthesize compound 7 with the following stoichiometric amounts; 1-(4-hydroxyphenyl)piperazine (0.30 g, 1.0 mmol), acetaminophen (0.15 g, 1.0 mmol), 37% formaldehyde (0.10 mL, 5 mmol) and 6,9- dichloroacridine (0.28 g, 1.0 mmol) to afford it as orange reddish semisolid (0.17 g) in 59 % yield; R_f 0.58 (1.5:8.5, MeOH:DCM); IR (cast film) ν_{\max} = 3334, 2918, 1737, 1564, 1468, 1235, 1181, 1031, 930, 830, 722 cm^{-1} ; ^1H NMR (500 MHz, CD_3OD) δ 8.07 (d, J = 9.3 Hz, 1H), 7.87 (d, J = 1.8 Hz, 1H), 7.82 (d, J = 9.3 Hz, 1H), 7.51– 7.46 (m, 1H), 7.41 (d, J = 2.5 Hz, 1H), 7.29 – 7.24 (m, 1H), 7.04 (dd, J = 8.7, 2.4 Hz, 1H), 6.93 – 6.89 (m, 1H), 6.88 – 6.81 (m, 3H), 6.70 (dd, J = 8.9, 2.3 Hz, 2H), 3.72 (s, 3H), 3.61 (s, 2H), 3.11 – 2.99 (m, 4H), 2.82 – 2.67 (m, 4H), OH and NH protons were not observed; ^{13}C NMR (125 MHz, CDCl_3) δ 156.3, 153.5, 152.1, 150.2, 150.1, 145.3, 145.2, 144.0, 125.3, 124.7, 122.5, 121.9, 121.5, 120.4, 120.0, 118.8 (2C), 118 (2C), 118.4, 118.1, 117.0, 116.5, 116.1, 115.9, 61.3, 55.4, 52.7 (2C), 50.7 (2C); HRMS (ESI) calcd for $\text{C}_{31}\text{H}_{30}\text{ClN}_4\text{O}_3$ $[\text{M} + \text{H}]^+$ 541.2001; found 541.2010.

4-((6-Chloro-2-methoxyacridin-9-yl)amino)phenol (8)

Synthesis of compound 8 was carried out according to the reported procedures ²¹ with minor modifications. The synthesis was performed by mixing 4-aminophenol (0.11 g, 1.0 mmol) and 6,9-dichloroacridine (0.28 g, 1.0 mmol) in 10 mL single neck round bottom flask and stirred at 90 °C under reflux. The course of reaction followed by TLC until little or no starting material was detected (around 12 h). On cooling to room temperature, the reaction mixture was diluted with cold water and neutralized to pH of 8-9 with 28% v/v ammonia solution. The alkaline solution was extracted with dichloromethane. The organic layer was washed with brine, concentrated in vacuum, and purified by column

1 chromatography (gradient elution with 1% to 5% MeOH:DCM system) to afford it as orange reddish
2 semisolid in 73 % yield; R_f 0.47 (1.5:8.5, MeOH:DCM); IR (cast film) ν_{\max} = 3325, 2918, 1737, 1562,
3 1468, 1236, 1180, 1103, 1050, 722 cm^{-1} ; ^1H NMR (500 MHz, CD_3OD) δ 8.12 (d, J = 9.4 Hz, 1H), 7.84
4 – 7.83 (m, 1H), 7.78 (d, J = 9.3 Hz, 1H), 7.61 (dd, J = 9.3, 2.6 Hz, 1H), 7.48 (d, J = 1.5 Hz, 1H), 7.35
5 (dd, J = 9.4, 2.1 Hz, 1H), 7.27 – 7.22 (m, 2H), 6.95 – 6.91 (m, 2H), 3.88 (s, 1H), 3.69 (s, 3H). OH proton
6 was not observed; ^{13}C NMR (125 MHz, CD_3OD) δ 158.9, 157.7, 141.7, 137.9, 133.2, 129.8, 128.4, 127.8
7 (2C), 126.6, 125.7, 122.2, 120.1, 119.3, 117.8 (2C), 116.1, 113.3, 104.5, 56.1.; HRMS (ESI) calcd for
8 $\text{C}_{20}\text{H}_{16}\text{ClN}_2\text{O}_2$ $[\text{M} + \text{H}]^+$ 351.0908; found 351.0896.

16 Molecular docking of compound 1

17
18
19
20 The first step of our VS study was to investigate the binding mode of the lead compound **1**²⁵ to the
21 pocket on the XPF C-terminus. We used twenty XPF structures as single targets for a relaxed complex
22 scheme (RCS) docking protocol, in order to accurately account for protein flexibility^{34, 35}. These
23 structures were extracted from the Protein Data Bank (PDB)³⁶ entry 1Z00¹⁷, reporting the NMR
24 ensemble of the dimerization complex between the ERCC1 and XPF HhH2 domains. The XPF structures
25 were optimized with a minimization process, details of which are reported in Supporting Information,
26 section 1.1. The binding site of each target was defined as the geometric center of the residues Y833,
27 N834, P837, Q838, M856, K860, N861 and I862 on the XPF HhH2 domain, as reported in our previous
28 study²⁵, where the residues are numbered according to the 1Z00 PDB file. Molecular docking
29 simulations were performed using the Lamarckian Genetic Algorithm (LGA)³⁷ and the built-in scoring
30 function³⁸ of Autodock4³⁹. Technical details regarding the docking simulations are reported in
31 Supporting Information, section 1.2.

32 Characterization of the binding pocket and pharmacophore modeling

33
34
35
36 To characterize the binding site and the binding mode of **1**, electrostatic maps were generated in the
37 MOE2015 software package⁴⁰, based on the docked pose of **1**, using -2 kcal/mol for the potential
38 isosurfaces of hydrophobic, acceptor and donor probe atoms, and the Poisson-Boltzmann equation to
39

1
2 compute the potentials. The maps were built within 4.5 Å of the ligand pose obtained from docking.
3
4 Using the information from the docking and electrostatic mapping, a pharmacophore model for **1** was
5
6 built with the MOE Pharmacophore Query Editor and the EHT scheme ⁴¹.
7
8
9

10 Docking-based virtual screening of compound **1** analogues

11
12
13 Fifty-seven analogues of compound **1** structure were designed by replacement of the piperazine N-methyl
14
15 group with other moieties expected to capture additional binding interactions of the piperazine ring. The
16
17 structures were prepared using Schrödinger LigPrep ⁴² to account for multiple tautomers, protonation
18
19 states and low-energy ring conformations, using the same approach as for **1** (Supporting Information,
20
21 section 1.2). The molecular docking simulations were performed with MOE Dock. Only the XPF
22
23 structure from the best compound **1** complex was used as a target for the VS study. Different
24
25 conformations of the analogues were obtained using Conformation Import. The previously built
26
27 pharmacophore model was used for the placement step, in which 30 poses are returned according to the
28
29 London dG scoring method ⁴³. To account for the local arrangement of the pocket residues upon ligand
30
31 binding, the Induced Fit method was selected for the refinement step, where the side chains of the binding
32
33 pocket were left to move freely. At the end, one pose scored with the Generalized Born Volume
34
35 Integral/Weighted Surface Area (GBVI/WSA) function was returned ⁴³. Water/octanol partition
36
37 coefficients (logP) of the molecules were calculated in MOE using the SlogP function ⁴⁴, which takes
38
39 into account the given protonation state of the molecule under examination. Ligand efficiencies were
40
41 calculated as the ratio between the computed binding energies and the number of heavy atoms of each
42
43 analog.
44
45
46
47
48
49
50

51 Molecular dynamics simulations and MM/GBSA rescoring of the analogues

52
53
54 To calculate an average binding energy for the hits, we performed 2 ns of MD simulations for the top
55
56 ranked compound-XPF complexes. Details of the preparation method and the parameters used in these
57
58

1 simulations are reported in Supporting Information, section 2.1. Free energy calculations were performed
2 over the trajectories with the MM/GBSA method, using the MMPBSA.py script ⁴⁵. For technical details
3 regarding the calculations refer to Supporting Information, section 2.1. The calculations were performed
4 on snapshots extracted every 10 ps from the MD trajectories, and per-residue decompositions of the
5 binding energies were also performed for the residues within 10 Å of any analog atom at the beginning
6 of the simulations. We also calculated the entropic contribution of ligand binding using the normal mode
7 analysis (NMA) method ⁴⁶. The final binding energies used to rank the compounds were calculated
8 combining the MM/GBSA and entropy contributions with the equation S1 in Supporting Information.
9
10
11
12
13
14
15
16
17
18
19
20

21 ERCC1-XPF protein preparation

22
23
24 Human ERCC1-XPF wild-type protein was obtained as previously described ²⁹. Basically, the
25 recombinant protein was expressed from a bicistronic plasmid (kindly provided by Dr. Richard Wood,
26 University of Texas MD Anderson Cancer Center, Smithville, TX) in the *E. coli* BL21 (DE3) strain.
27 Since both XPF and ERCC1 contained a polyhistidine (His-6) tag, the proteins extracted from *E. coli*
28 were incubated with a ProBond Nickel-Chelating Resin (Thermo Fisher Scientific). Protein eluted from
29 the Ni affinity column was subsequently loaded into a Hi-trap heparin column (GE Healthcare). Fractions
30 recovered from the heparin column that contained ERCC1-XPF were dialyzed, concentrated and stored
31 at -80°C in 10 mM HEPES pH 7.4, 2.5 mM β-mercaptoethanol, 0.01% CHAPS, 0.25 mM EDTA, 50%
32 glycerol and 25 mM NaCl.
33
34
35
36
37
38
39
40
41
42
43
44
45

46 Microplate fluorescence incision assay

47
48
49 We followed a previously described protocol ^{2, 29}. Briefly, reactions were carried out in 384-well black,
50 flat-bottomed microtiter plates (OptiPlate – 384 F, Perkin Elmer) in a total volume of 20 µl containing
51 the indicated concentrations of inhibitor compounds, 100 nM stem-loop substrate [6-FAM-5'-
52 CAGCGCTCGG(20T)CCGAGCGCTG-3'-dabcyl], 25 ng ERCC1-XPF, 50 mM Tris-Cl pH 8, 20 mM
53
54
55
56
57
58
59
60

1 NaCl, 0.5 mM DDT and 0.75 mM MnCl₂ at 25°C. Fluorescent readings were obtained using a FLUOstar
2
3
4 Optima fluorimeter (BMG Labtech) with Optima software at an excitation of and emission wavelengths
5
6 of 485 and 520 nm respectively, for 12 minutes.
7
8
9

10 Steady-state fluorescence assays

11
12
13 Steady-state fluorescence spectra were measured at room temperature on a Perkin-Elmer LS-55
14
15 spectrofluorometer (Freemont, CA) with 5 nm spectral resolution for excitation and emission using 30-
16
17 80 nM solution of purified recombinant ERCC1-XPF protein complex. Protein fluorescence was excited
18
19 at 295 nm, and fluorescence emission spectra were recorded in the 300-400 nm range: changes in
20
21 fluorescence intensity was monitored at the emission maximum (330 nm). In studying the effects of
22
23 inhibitors on protein fluorescence intensities, additions to protein samples were made from inhibitors
24
25 stock solutions, keeping the protein dilution below 3%.
26
27
28
29

30 Expression and purification of recombinant truncated forms of ERCC1 and XPF:

31
32 Synthetic DNA sequences encoding for human ERCC1 codons 96-297 (dERCC1) and XPF codons 667-
33
34 916 (dXPF) inserted into separate pET-28a expression plasmids were used to transform BL21(DE3) cells
35
36 and express the corresponding recombinant proteins ². Since the truncated form of the proteins both
37
38 contained N-terminal polyhistidine-tags (His-tags) they were purified utilizing a nickel-chelating resin
39
40 (ThermoFisher Scientific) under conditions similar to the ones described ². Both truncated peptides were
41
42 finally solubilized to final concentrations for the experiments of 40 nM dXPF and 20 nM dERCC1 in a
43
44 buffer (MST buffer) containing: 20 mM HEPES pH 7.4, 50 mM NaCl, 1 mM DTT, 2 mM MgCl₂, 5%
45
46 glycerol and 0.01% CHAPS.
47
48
49

50 Microscale thermophoresis (MST) measurements

51
52
53 We tried to remove the His-tag from one of the truncated peptides (preferentially dERCC1 because of its
54
55 low yield) to carry out MST equilibrium experiments. However, the peptides proved to be resistant to
56
57
58
59
60

1
2 thrombin treatment so, we decided to follow a different qualitative approach. Both, dXPF and dERCC1
3
4 were labelled with 20 nM and 10 nM RED-tris-NTA (NanoTemper Technologies), respectively,
5
6 following the manufacturer instructions. Individual peptides (20 nM final concentration) or equimolar
7
8 amounts of dERCC1 and dXPF (20 nM final concentration of the dimer) were incubated in MST buffer
9
10 in the presence of compound **4** (10 μ M) or DMSO. After 20 minutes of incubation time at room
11
12 temperature 10 μ l of the samples were placed in standard capillaries (NanoTemper Technologies) and
13
14 the emitted red fluorescence (670 nm) was measured in a Monolith NT.115 instrument (NanoTemper
15
16 Technologies) with a High MST-Power, 70% Excitation Power and a Nano-RED Excitation type. Pretest
17
18 and binding check experiments did not show any change in fluorescence of the RED-tris-NTA dye
19
20 induced by compound **4**. In addition, the peak shape did not indicate any adsorption of the components
21
22 of the solution to the surface of the capillaries.
23
24
25
26
27

28 Cell culture

29
30
31 The human colorectal cancer HCT-116 cell line was obtained from the American Type Culture
32
33 Collection (ATCC). The cell population was expanded immediately after arrival, aliquoted and stored
34
35 frozen in liquid nitrogen. Freshly thawed cells were used for each experiment. The cells were cultured in
36
37 a 1:1 DMEM/F12 media supplemented with 10% FBS, 50 units/mL penicillin, 50 μ g/mL streptomycin,
38
39 mM l-glutamine, 0.1 mM nonessential amino acids, 1 mM sodium pyruvate and maintained under 5%
40
41 CO₂ in a humidifier incubator at 37°C. All the supplies for cell culture were obtained from Gibco/BRL.
42
43
44
45

46 Cellular repair of cyclobutane pyrimidine dimers

47
48
49 We followed the protocol of Mirzayans *et al.* with minor modifications³³. Approximately 1 x 10⁵ HCT-
50
51 116 cells were seeded on each coverslip and allowed to attach overnight. Medium was then removed and
52
53 cells were treated for one hour with the desired compound. The medium was removed, and cells were
54
55 exposed to 8 J/m² UV-C radiation (G15T8 254 nm lamp, Ushio America Inc, Cypress, CA) followed by
56
57
58
59
60

1
2 adding fresh medium containing the compound. Plates were incubated at 37°C for different periods of
3
4 time up to 24 hours and fixed in 50:50 methanol/1X phosphate-buffered saline (PBS) solution, followed
5
6 by replacing the methanol/PBS solution with 100% methanol and incubation in -20°C. After 20 minutes,
7
8 methanol was removed, and cells were treated with PBS for 5 minutes in room temperature. After fixing,
9
10 cells were permeabilized in 0.5% Triton/PBS and washed with PBS, denatured in 2 N HCl, and
11
12 neutralized by twice washing with 0.1 M borate buffer pH 8.5. Cells on cover slips were washed once
13
14 with PBS followed by blocking with 5% non-fat dry milk/PBS for 30 minutes. Mouse anti-thymine dimer
15
16 monoclonal antibody (Cat. No. MC-062, Kamiya Biomedical Company, Seattle, WA) was applied to the
17
18 cover slips for one hour in the dark and at room temperature. Cells were then washed with PBS containing
19
20 0.1% Tween-20 and incubated with rabbit anti-mouse IgG-Alexafluor antibody (Invitrogen, Carlsbad,
21
22 CA) followed by two washes with PBS/(0.1%)Tween-20. Cells on coverslips were then washed with
23
24 PBS, rinsed with water, and mounted on slides using DAPI glycerol mounting solution. Slides were kept
25
26 at 4°C before fluorescent microscopic evaluation and measurement of fluorescence intensity with
27
28 MetaXpress Version: 6.2.1.704 software (Molecular Devices, Sunnyvale, California).
29
30
31
32
33

34 Clonogenic survival assay

35
36
37
38 UV treatment: HCT-116 cells (100-800 cells depending on the UV dose) were plated in triplicate in 60-
39
40 mm petri dishes. The cells were incubated overnight at 37°C in a humidified atmosphere containing 5%
41
42 CO₂ to allow for cell attachment. Medium was then removed, and cells were treated with 1 or 2 μM
43
44 compound **4** for one hour. Medium was removed again, and cells were exposed to increasing doses (0-
45
46 10 J/m²) of UV-C radiation and then incubated for a further 10 days in the presence of inhibitor at 37°C
47
48 in a 5% CO₂ atmosphere to allow for colony formation. After this period plates were stained with crystal
49
50 violet and colonies were counted using a Colcount instrument (Oxford Optronix, Abingdon UK). Finally,
51
52 plating efficiency and surviving fraction were calculated.
53
54
55
56
57
58
59
60

1
2 Cyclophosphamide treatment: A similar protocol was followed as described for the UV treatment, except
3
4 that cells were treated with 1 or 2 μM compound **4** for 4 hours followed by addition of increasing doses
5
6 of cyclophosphamide (0-300 μM). After 24 hours medium was replaced with fresh medium containing
7
8 compound **4** alone. Plates were incubated for another 8 days at 37°C in a 5% CO₂ atmosphere for colony
9
10 formation. After this period plates were stained with crystal violet, colonies were counted, and plating
11
12 efficiency and surviving fraction were calculated.
13
14
15

16 PK assessment of compound **4** and Compound **1**

17
18
19
20 Standard protocols were used for assessing the absorption, distribution, metabolism and excretion
21
22 (ADME) profile of our lead compound **4** and compound **1** (reference hit). Screening were performed at
23
24 WuXi AppTec (Shanghai) Co (Please add the website as a new reference: <https://www.wuxiapptec.com/>)
25
26 to conduct the following assays according to the standard protocols; Distribution coefficient (Log D at
27
28 pH 7.4), aqueous solubility (Kinetic), metabolic stability in human liver microsomes and cryopreserved
29
30 human hepatocytes, bidirectional permeability in Caco-2 cells, serum protein binding, and cytochromes
31
32 P450 (CYPs) inhibition (CYP1A2, CYP2C9, CYP2C19, CYP2D6, CYP3A4-M).
33
34
35

36 **Ancillary Information**

37
38
39 **Supporting Information:** Molecular docking of compound **1**, MD simulations and MM/GBSA rescoring
40
41 of the analogues; synthesis scheme of compound **1** analogues; cell proliferation assay, virtual screening
42
43 of compound **1** analogues; computational results for the subset of analogues chosen for synthesis; half-
44
45 maximum inhibitory concentrations for the compounds with the highest inhibitor potential;
46
47 pharmacokinetic profile of compound **4** and compound **1**; synthesis and characterization of inhibitors (**1**-
48
49 **8**); cytotoxicity profile of compound **4** and compound **5**, microscale measurements (MST); ¹H/¹³C NMR
50
51 spectra of compounds; HPLC chromatogram of compound **4**. Molecular formula strings.
52
53
54
55

56
57 **Corresponding Author Information:** fwest@ualberta.ca
58
59

1
2
3
4 **Acknowledgments:** This work was supported by the Alberta Cancer Foundation Transformative Program
5
6 Project (26603) awarded to JAT, MW and FGW. AHE was supported by a Marshall Syska Scholarship.
7
8 FG was supported by an Alberta Innovates Graduate Student Scholarship. All the computational work
9
10 was performed on Pharmamatrix cluster.
11
12

13
14 **Author Contributions:** All authors have given approval to the final version of the manuscript. A.E.
15
16 designed and wrote the manuscript, synthesized and characterized all the compounds; F.G. designed the
17
18 computational studies of the compounds and helped in mastering some of the graphs. D.J. expressed and
19
20 purified ERCC1-XPF, employed the *in vitro* ERCC-XPF1 assay and conducted microscale
21
22 thermophoresis measurements. F.K.B and Y.X. carried out cell culture, UV dimer repair assay and
23
24 clonogenic survival assay. O.S helped in mentoring A.E in the synthesis and characterization of the
25
26 compounds. C.W. was responsible for purification and HPLC analysis of compound 4. R.M conducted
27
28 the binding affinity studies of the compounds. K.B. and J.T. were supervising F.G. in designing VS
29
30 studies. M.W. and F.W. drafted the manuscript.
31
32
33
34
35
36
37

38 **Funding Sources:** AHE was supported by a Marshall Syska Scholarship, FG was supported by an
39
40 Alberta Innovates Graduate Student Scholarship. This work was supported by the Alberta Cancer
41
42 Foundation Transformative Program Project (26603) to JAT, MW and FGW
43
44
45
46

47 **Conflict of Interest:** The authors declare no conflicts of interests.
48
49
50

51 **Abbreviations:** CPDs, cyclobutane pyrimidine dimers; VS, virtual screening; MMC, cyclophosphamide
52
53 and mitomycin C ; HhH2, helix–hairpin–helix; MD, molecular dynamics; EDG, electron donating group;
54
55
56
57
58
59
60

EWG, electron withdrawing group; HBA, hydrogen bond acceptor; WT, wild type cells; CYP, cytochrome P enzyme; ICL, interstrand crosslink; SAR, structure activity relationship.

References

1. Sijbers, A. M.; de Laat, W. L.; Ariza, R. R.; Biggerstaff, M.; Wei, Y.-F.; Moggs, J. G.; Carter, K. C.; Shell, B. K.; Evans, E.; de Jong, M. C. Xeroderma pigmentosum group F caused by a defect in a structure-specific DNA repair endonuclease. *Cell* **1996**, *86*, 811-822.
2. McNeil, E. M.; Astell, K. R.; Ritchie, A.-M.; Shave, S.; Houston, D. R.; Bakrania, P.; Jones, H. M.; Khurana, P.; Wallace, C.; Chapman, T.; Wear, M. A.; Walkinshaw, M. D.; Saxty, B.; Melton, D. W. Inhibition of the ERCC1–XPF structure-specific endonuclease to overcome cancer chemoresistance. *DNA Repair* **2015**, *31*, 19-28.
3. Friedberg, E. C.; Walker, G. C.; Siede, W.; Wood, R. D.; Schultz, R. A.; Ellenberger, T. In *DNA Repair and Mutagenesis*. 2nd edn ASM Press. American Society of Microbiology, Washington, DC **2006**.
4. McNeil, E. M.; Melton, D. W. DNA repair endonuclease ERCC1–XPF as a novel therapeutic target to overcome chemoresistance in cancer therapy. *Nucleic Acids Res.* **2012**, *40*, 9990-10004.
5. Douwel, D. K.; Hoogenboom, W. S.; Boonen, R. A. C. M.; Knipscheer, P. Recruitment and positioning determine the specific role of the XPF-ERCC1 endonuclease in interstrand crosslink repair. *EMBO J.* **2017**, *36*, 2034-2046.
6. Yagi, T.; Katsuya, A.; Koyano, A.; Takebe, H. Sensitivity of group F xeroderma pigmentosum cells to UV and mitomycin C relative to levels of XPF and ERCC1 overexpression. *Mutagenesis* **1998**, *13*, 595-599.
7. Gajjar, K. K.; Yadav, D. K.; Kobawala, T. P.; Trivedi, T. I.; Vora, H. H.; Ghosh, N. R. ERCC1 expression in patients with colorectal cancer: a pilot study. *J. Cancer Metastasis Treat.* **2016**, *2*, 471-476.
8. McHugh, P. J.; Spanswick, V. J.; Hartley, J. A. Repair of DNA interstrand crosslinks: molecular mechanisms and clinical relevance. *Lancet Oncol.* **2001**, *2*, 483-490.
9. Ahmad, A.; Robinson, A. R.; Duensing, A.; van Drunen, E.; Beverloo, H. B.; Weisberg, D. B.; Hastly, P.; Hoeijmakers, J. H. J.; Niedernhofer, L. J. ERCC1-XPF endonuclease facilitates DNA double-strand break repair. *Mol. Cell. Biol.* **2008**, *28*, 5082-5092.
10. de Laat, W. L.; Appeldoorn, E.; Jaspers, N. G. J.; Hoeijmakers, J. H. J. DNA structural elements required for ERCC1-XPF endonuclease activity. *J. Biol. Chem.* **1998**, *273*, 7835-7842.
11. Gaillard, P.-H. L.; Wood, R. D. Activity of individual ERCC1 and XPF subunits in DNA nucleotide excision repair. *Nucleic Acids Res.* **2001**, *29*, 872-879.

12. Gentile, F.; Tuszynski, J. A.; Barakat, K. H. New design of nucleotide excision repair (NER) inhibitors for combination cancer therapy. *J. Mol. Graphics Modell.* **2016**, *65*, 71-82.
13. Gentile, F.; Barakat, K. H.; Tuszynski, J. A. Computational Characterization of Small Molecules Binding to the Human XPF Active Site and Virtual Screening to Identify Potential New DNA Repair Inhibitors Targeting the ERCC1-XPF Endonuclease. *Int. J. Mol. Sci.* **2018**, *19*, 1328-1341.
14. Gentile, F.; Tuszynski, J.; Barakat, K. Modelling DNA repair pathways: recent advances and future directions. *Curr. Pharm. Des.* **2016**, *22*, 3527-3546.
15. Ahmad, A.; Enzlin, J. H.; Bhagwat, N. R.; Wijgers, N.; Raams, A.; Appeldoorn, E.; Theil, A. F.; Hoeijmakers, J. H. J.; Vermeulen, W.; Jaspers, N. G. J. Mislocalization of XPF-ERCC1 nuclease contributes to reduced DNA repair in XP-F patients. *PLoS Genet.* **2010**, *6*, 1000871-1000882.
16. de Laat, W. L.; Sijbers, A. M.; Odijk, H.; Jaspers, N. G. J.; Hoeijmakers, J. H. J. Mapping of interaction domains between human repair proteins ERCC1 and XPF. *Nucleic Acids Res.* **1998**, *26*, 4146-4152.
17. Tripsianes, K.; Folkers, G.; Eiso, A. B.; Das, D.; Odijk, H.; Jaspers, N. G. J.; Hoeijmakers, J. H. J.; Kaptein, R.; Boelens, R. The structure of the human ERCC1/XPF interaction domains reveals a complementary role for the two proteins in nucleotide excision repair. *Structure* **2005**, *13*, 1849-1858.
18. Choi, Y.-J.; Ryu, K.-S.; Ko, Y.-M.; Chae, Y.-K.; Pelton, J. G.; Wemmer, D. E.; Choi, B.-S. Biophysical characterization of the interaction domains and mapping of the contact residues in the XPF-ERCC1 complex. *J. Biol. Chem.* **2005**, *280*, 28644-28652.
19. Tsodikov, O. V.; Enzlin, J. H.; Schärer, O. D.; Ellenberger, T. Crystal structure and DNA binding functions of ERCC1, a subunit of the DNA structure-specific endonuclease XPF-ERCC1. *Proc. Natl. Acad. Sci. U. S. A.* **2005**, *102*, 11236-11241.
20. McNeil, E. M.; Astell, K. R.; Ritchie, A.-M.; Shave, S.; Houston, D. R.; Bakrania, P.; Jones, H. M.; Khurana, P.; Wallace, C.; Chapman, T. Inhibition of the ERCC1-XPF structure-specific endonuclease to overcome cancer chemoresistance. *DNA Repair* **2015**, *31*, 19-28.
21. Chapman, T. M.; Gillen, K. J.; Wallace, C.; Lee, M. T.; Bakrania, P.; Khurana, P.; Coombs, P. J.; Stennett, L.; Fox, S.; Bureau, E. A. Catechols and 3-hydroxypyridones as inhibitors of the DNA repair complex ERCC1-XPF. *Bioorg. Med. Chem. Lett.* **2015**, *25*, 4097-4103.
22. Chapman, T. M.; Wallace, C.; Gillen, K. J.; Bakrania, P.; Khurana, P.; Coombs, P. J.; Fox, S.; Bureau, E. A.; Brownlees, J.; Melton, D. W. N-Hydroxyimides and hydroxypyrimidinones as inhibitors of the DNA repair complex ERCC1-XPF. *Bioorg. Med. Chem. Lett.* **2015**, *25*, 4104-4108.
23. Arora, S.; Heyza, J.; Zhang, H.; Kalman-Maltese, V.; Tillison, K.; Floyd, A. M.; Chalfin, E. M.; Bepler, G.; Patrick, S. M. Identification of small molecule inhibitors of ERCC1-XPF that inhibit DNA repair and potentiate cisplatin efficacy in cancer cells. *Oncotarget* **2016**, *7*, 75104-75117.

- 1
2 24. Yang, L.; Ritchie, A.-M.; Melton, D. W. Disruption of DNA repair in cancer cells by
3 ubiquitination of a destabilising dimerization domain of nucleotide excision repair protein
4 ERCC1. *Oncotarget* **2017**, *8*, 55246-55264.
5
6 25. Jordheim, L. P.; Barakat, K. H.; Heinrich-Balard, L.; Matera, E.-L.; Cros-Perrial, E.; Bouledrak,
7 K.; El Sabeh, R.; Perez-Pineiro, R.; Wishart, D. S.; Cohen, R. Small molecule inhibitors of
8 ERCC1-XPF protein-protein interaction synergize alkylating agents in cancer cells. *Mol.*
9 *Pharmacol.* **2013**, *84*, 12-24.
10
11 26. Chapman, T. M.; Gillen, K. J.; Wallace, C.; Lee, M. T.; Bakrania, P.; Khurana, P.; Coombs, P.
12 J.; Stennett, L.; Fox, S.; Bureau, E. A.; Brownlees, J.; Melton, D. W.; Saxty, B. Catechols and 3-
13 hydroxypyridones as inhibitors of the DNA repair complex ERCC1-XPF. *Bioorg. Med. Chem.*
14 *Lett.* **2015**, *25*, 4097-4103.
15
16 27. Arora, S.; Heyza, J.; Zhang, H.; Kalman-Maltese, V.; Tillison, K.; Floyd, A. M.; Chalfin, E. M.;
17 Bepler, G.; Patrick, S. M. Identification of small molecule inhibitors of ERCC1-XPF that inhibit
18 DNA repair and potentiate cisplatin efficacy in cancer cells. *Oncotarget* **2016**, *46*, 75104-75117.
19
20 28. Scurr, M.; Pembroke, T.; Bloom, A.; Roberts, D.; Thomson, A.; Smart, K.; Bridgeman, H.;
21 Adams, R.; Brewster, A.; Jones, R.; Gwynne, S.; Blount, D.; Harrop, R.; Hills, R.; Gallimore, A.;
22 Godkin, A. Low-Dose Cyclophosphamide Induces Antitumor T-Cell Responses, which Associate
23 with Survival in Metastatic Colorectal Cancer. *Clin. Cancer Res.* **2017**, *23*, 6771-6780.
24
25 29. Bowles, M.; Lally, J.; Fadden, A. J.; Mouilleron, S.; Hammonds, T.; McDonald, N. Q.
26 Fluorescence-based incision assay for human XPF-ERCC1 activity identifies important elements
27 of DNA junction recognition. *Nucleic Acids Res.* **2012**, *40*, 101-113.
28
29 30. Jerabek-Willemsen, M.; Wienken, C. J.; Braun, D.; Baaske, P.; Duhr, S. Molecular interaction
30 studies using microscale thermophoresis. *Assay Drug Dev. Technol.* **2011**, *9*, 342-353.
31
32 31. Wienken, C. J.; Baaske, P.; Rothbauer, U.; Braun, D.; Duhr, S. Protein-binding assays in
33 biological liquids using microscale thermophoresis. *Nat. Commun.* **2010**, *1*, 100-107.
34
35 32. Zillner, K.; Jerabek-Willemsen, M.; Duhr, S.; Braun, D.; Längst, G.; Baaske, P. Microscale
36 thermophoresis as a sensitive method to quantify protein: nucleic acid interactions in solution.
37 *Funct. Genomics* **2012**, *815*, 241-252.
38
39 33. Mirzayans, R.; Pollock, S.; Scott, A.; Gao, C. Q.; Murray, D. Metabolic labeling of human cells
40 with tritiated nucleosides results in activation of the ATM-dependent p53 signaling pathway and
41 acceleration of DNA repair. *Oncogene* **2003**, *22*, 5562-5571.
42
43 34. Philippopoulos, M.; Lim, C. Exploring the dynamic information content of a protein NMR
44 structure: Comparison of a molecular dynamics simulation with the NMR and X-ray structures
45 of Escherichia coli ribonuclease HI. *Proteins: Struct., Funct., Bioinf.* **1999**, *36*, 87-110.
46
47 35. Ishima, R.; Torchia, D. A. Protein dynamics from NMR. *Nat. Struct. Mol. Biol.* **2000**, *7*, 740-743.
48
49 36. Berman, H. M.; Westbrook, J.; Feng, Z.; Gilliland, G.; Bhat, T. N.; Weissig, H.; Shindyalov, I.
50 N.; Bourne, P. E. The Protein Data Bank. *Nucleic Acids Res.* **2000**, *28*, 235-242.
51
52
53
54
55
56
57
58
59
60

- 1
2 37. Morris, G. M.; Goodsell, D. S.; Halliday, R. S.; Huey, R.; Hart, W. E.; Belew, R. K.; Olson, A.
3 J. Automated docking using a Lamarckian genetic algorithm and an empirical binding free energy
4 function. *J. Comput. Chem.* **1998**, 19, 1639-1662.
5
6 38. Huey, R.; Morris, G. M.; Olson, A. J.; Goodsell, D. S. A semiempirical free energy force field
7 with charge-based desolvation. *J. Comput. Chem.* **2007**, 28, 1145-1152.
8
9 39. Morris, G. M.; Huey, R.; Lindstrom, W.; Sanner, M. F.; Belew, R. K.; Goodsell, D. S.; Olson, A.
10 J. AutoDock4 and AutoDockTools4: Automated docking with selective receptor flexibility. *J.*
11 *Comput. Chem.* **2009**, 30, 2785-2791.
12
13 40. Chemical Computing Group, I. *Molecular Operating Environment (MOE)*, 2013.08; **2017**.
14
15 41. Lin, A. Overview of Pharmacophore Applications in MOE.
16 <https://www.chemcomp.com/journal/ph4.htm> (accessed Jun 15, 2019).
17
18 42. LigPrep, Schrödinger LLC: New York, NY **2013**.
19
20 43. Labute, P. The generalized Born/volume integral implicit solvent model: estimation of the free
21 energy of hydration using London dispersion instead of atomic surface area. *J. Comput. Chem.*
22 **2008**, 29, 1693-1698.
23
24 44. Wildman, S. A.; Crippen, G. M. Prediction of physicochemical parameters by atomic
25 contributions. *J. Chem. Inf. Comput. Sci.* **1999**, 39, 868-873.
26
27 45. Miller Iii, B. R.; McGee Jr, T. D.; Swails, J. M.; Homeyer, N.; Gohlke, H.; Roitberg, A. E.
28 MMPBSA. py: an efficient program for end-state free energy calculations. *J. Chem. Theory*
29 *Comput.* **2012**, 8, 3314-3321.
30
31 46. Kassem, S.; Ahmed, M.; El-Sheikh, S.; Barakat, K. H. Entropy in bimolecular simulations: A
32 comprehensive review of atomic fluctuations-based methods. *J. Mol. Graphics Modell.* **2015**, 62,
33 105-117.
34
35
36
37
38
39
40
41
42
43
44
45
46
47
48
49
50
51
52
53
54
55
56
57
58
59
60

Table of Content Graphic

